

We are IntechOpen, the world's leading publisher of Open Access books Built by scientists, for scientists

6,900

Open access books available

186,000

International authors and editors

200M

Downloads

Our authors are among the

154

Countries delivered to

TOP 1%

most cited scientists

12.2%

Contributors from top 500 universities



WEB OF SCIENCE™

Selection of our books indexed in the Book Citation Index
in Web of Science™ Core Collection (BKCI)

Interested in publishing with us?
Contact book.department@intechopen.com

Numbers displayed above are based on latest data collected.
For more information visit www.intechopen.com



Tidal Evolution Related to Changing Sea Level; Worldwide and Regional Surveys, and the Impact to Estuaries and Other Coastal Zones

Adam Thomas Devlin and Jiayi Pan

Abstract

Global sea level rise understanding is critical for coastal zones, and estuaries are particularly vulnerable to water level changes. Sea level is increasing worldwide due to several climactic factors, and tidal range may also change in estuaries due to sea level rise and anthropogenic harbor improvements that may modify friction and resonance, increasing risks to population centers. Tidal range changes may further complicate the risks of sea level rise, increasing the frequency of nuisance flooding, and may affect tide-sensitive ecosystems. Higher total water levels threaten to increase flood zone areas in estuarine regions, which can impact the infrastructure, industry, and public health of coastal populations, as well as disrupting sensitive biological habitats. Therefore, it is of critical interest to analyze how tidal range changes under sea level changes. This chapter describes the tidal anomaly correlation (TAC) methodology which can quantify the tidal evolution related to sea level changes. A basin-wide survey of Pacific and Atlantic Ocean tide gauges is detailed, showing that tidal changes due to sea level rise is present at most locations surveyed. A focused regional study of Hong Kong is also described as an example of how tidal evolution can impact high population density coastal zones.

Keywords: ocean tides, tidal variability, sea level rise, coastal flooding, nuisance flooding

1. Introduction

Ocean tides are a manifestation of the response to the gravitational forcing induced by astronomical bodies; namely, the Sun and Moon. The lunar forcing is approximately twice the magnitude of the solar forcing, since the closer distance of the Moon is more important than the larger mass of the Sun, as the universal law of gravitation is directly proportional to mass but inversely proportional to the square of the distance between heavenly bodies. However, there are also interactions between the Sun and Moon that modulate the distance of both bodies, which in turn influences the forcing felt at any point on Earth as a linear combination of tidal

frequencies with forcing frequencies that range from twice-daily to decadal. Thus, though gravitation between two bodies is straightforward and definite, the true expression of tidal forcing experienced on Earth is an example of complex relation known as the “three-body problem” [1], which is only numerically calculable. However, this forcing is well-known, and essentially constant over short timescales.

Logic would dictate that due to this predictable “celestial clockwork”, the ocean tides on Earth should be equally predictable at all locations. However, this would only be true if Earth’s oceans had a constant depth and simple coastlines, as originally assumed by LaPlace in his tidal equations in the eighteenth century. This, of course, is not the case. Earth has a complex and highly variable ocean depth, with undersea ridges, trenches, plateaus, and valleys. Coastlines are also highly complex. Both factors can modulate the response of tidal forcing, with shallow coastal areas being the most sensitive. Thus, coastal tides are much larger and more variable than those seen in the deep ocean. The tides in coastal regions are also highly sensitive to changes in the shape and depth of shallow water regions. Some semi-enclosed coastal regions can amplify the resonant response of tidal forcing, such as in the Bay of Fundy in Canada, where tides can exceed tens of meters. Changes in local water depth can also influence the response of tides. Since recent decades have experienced the most rapid rise in mean sea levels (MSL) in millennia [2, 3], due to the steric rise of the ocean from ice melt and the thermal expansion of ocean water [4], both due to climate-change induced factors, future tidal range evolution is likely.

The changes in MSL are most pronounced in shallow coastal regions, especially in developed population centers, such as estuaries. Changes in MSL may lead to a change in local water depth in coastal regions, which have a first-order impact to coastal zones as rising background water levels. In turn, changes in water depth can modulate the response of tides as the resonant behavior changes. Small changes in water depth can lead to large changes in tidal range, which leads to a second-order impact to coastal zones. Estuaries are among the most vulnerable areas to these changes, since these regions are where large population centers are located, as well as sensitive ecosystems. Both natural and anthropogenic systems are highly dependent on tides. Biological habitats such as mangrove forests rely on constant tidal range, as do the complex food webs seen in estuarine regions. Consequently, changes in biology and ecology can have serious detrimental effects on human society, as much of the economy and industry of estuarine population may be dependent on stable ecosystems, e.g., fisheries, farming, and tourism. Changes in tidal range, tidal currents and tidal energy distribution can amplify these factors.

There are significant physical risks to estuarine cities and population centers that can be brought about by changing tides related to MSL rise. A large percentage of human settlements are in estuarine regions, as the abundance of fresh water and easy access to the open ocean allows civilization to easily thrive in these regions. Throughout history, estuarine cities have existed at the mercy of both the river and the sea. Extreme floods or extreme droughts can lead to extreme responses of the riverine aspects of estuaries, with implications for local farming and public health factors. On the oceanic side, storm events such as hurricanes and typhoons or tsunamis can be disastrous to estuarine cities, with extensive infrastructure damage and disruption to the local economy. However, both types of extreme events tend to be short-lived, and population centers in estuaries have developed knowing that even though such events can happen anytime, the average properties of the coastal zones, such as mean sea level and local tidal range, remain relatively constant. These assumptions have determined the planning and design of estuarine developments, such as harbors, roads, residence centers, and other infrastructure. Flooding due to inland storms and river surge might be occasionally extreme, but it could be

predicted to only reach certain maximum flood levels. However, under scenarios of sea level rise, and the resultant changes in ocean tides, modern times are now producing changes in this “stable background”, and previous assumptions of the worst-case scenarios may no longer be valid, rendering past coastal defense efforts inadequate to resist future extreme events. Changing tides on top of sea-level rise also allow the possibility of nuisance flooding, also known as “sunny-day flooding”, in which flood levels can be exceeded at exceptional high tides without the influence of a storm or river surge event [5, 6]. Other impacts possible under rising sea-levels and tidal evolution besides local flooding include disruptions in shipping and other coastal-based logistic factors. Most importantly, the coupled changes in MSL and ocean tides may be occurring rapidly, and across multiple spatial and temporal scales, making it a complex problem to predict with certainty, as each coastal location may experience a much different response.

This chapter will explore the dynamics and details of changing ocean tides. A background will first be given about past research that has identified secular (long-term) non-astronomical changes in ocean tides as well as a summary of past studies of MSL rise. Next will be a description of the methodology of newer efforts that have analyzed the correlated changes in sea levels and ocean tides in the Pacific and Atlantic Oceans, based primarily on the work of Devlin et al. [7–11]. Following this will be a summary of significant results in the Pacific and Atlantic basins, as well as results from a focused study of the Hong Kong region, where some of the strongest magnitude changes have been observed. Next, there will be a discussion section about the implications of coupled MSL and tidal variability for estuaries and coastal zones including effects like nuisance flooding, and finally, conclusions.

2. Background

2.1 Sea level changes

Mean sea level (MSL) is increasing nearly everywhere on Earth, with a globally-averaged rise of $+1.7 \pm 0.2 \text{ mm year}^{-1}$ as estimated from coastal and island tide gauge measurements from 1900 to 2009 [2, 12, 13], and at a rate $+3.4 \pm 0.4 \text{ mm year}^{-1}$ for 1993–2016 as estimated from satellite altimetry (<http://sealevel.colorado.edu/>; [14]). In the twentieth century, the most rapid increase in MSL over the last three millennia has been observed, based on a semi-empirical estimate of sea-level rise [3], finding that without global warming, the observed increases in global sea levels would have been much less. Furthermore, since ~1970, global mean sea level rise has been dominated by anthropogenic forcing [15]. Some climate models predict that MSL rates will accelerate in future decades via global climate change mechanisms [13] such as ice sheet melt and thermohaline MSL rise; both of these are induced by upper-ocean warming [4, 12, 16–19].

However, there is a wide spatial variability to these rates [3, 20], attributed to the combined effects of spatially variable wind and warming, and different vertical rates of land subsidence. In the Western Pacific, MSL rise often is larger than $+10 \text{ mm year}^{-1}$ in some locations, whereas Eastern Pacific rates are near zero or sometimes slightly negative because of tectonic and weather factors [21]. The anomalously rapid sea level rise observed in the western Pacific tends to be underestimated in many models. This may be because of low variability in tropical zonal wind stress [22]. However, the extreme rate in the Western tropical Pacific is unlikely to persist unabated [23], and a reversal of this Pacific asymmetry may be imminent soon.

2.2 Tidal changes

Ocean tides have classically been considered stationary because of their close relationship to celestial motion of the Moon and Sun [24]. However, many studies have clearly demonstrated that tides are evolving at different rates in different regions of the world, and these changes are not related to astronomical forcing [25–28]. Early studies discovered that long-term tidal changes are present at some stations such as at Brest, France, which has been steadily recording tidal levels for hundreds of years [29, 30]. It has also been shown that tidal changes can be a result of harbor modifications [31–36] through mechanisms such as channel deepening and land reclamation. Alternatively, long-term tidal changes can be due to modulations in the internal tide [37, 38]. Regionally focused studies have discovered changes in the major diurnal and semidiurnal tides in the Eastern Pacific [39], in the Gulf of Maine, [40], in the North Atlantic [26, 41], in China [42, 43], in Japan [44], and at certain Pacific islands [45].

2.3 Coupled changes in tides and MSL

Mean sea levels may influence tidal evolution directly, or it may be correlated with tidal variability through secondary mechanisms in a multitude of ways; some may be acting locally, and others may be active on basin-wide (amphidromic) scales. One way is through changes in water depth (e.g., due to climate-change induced sea level rise), which may influence tides on a large geographic scale via a “coupled oscillator” mechanism between the shelf and the deep ocean [46, 47]. Water depth changes can also modify the propagation and dissipation of tides [48, 49] by directly altering wave speed in shallow areas, or by changing the effect of bottom friction. The warming of the upper ocean [4] may lead to internal changes to stratification properties and a modulation of thermocline depth. Both mechanisms can yield a steric sea level signal which may modify the surface manifestation of internal tides, thus producing a detectable change at tide gauges. Such changes have been observed at the Hawaiian Islands [37]. On a shorter timescale, seasonal tidal variations can be due to rapid changes in water column stratification [50, 51], or by seasonal river flow characteristics [52, 53]. The shifting of the amphidromic points, e.g., as seen around Britain and Ireland [54], is possibly associated with changes in regional tidal properties [55]. In harbors and estuaries, increased water depths can alter the tidal prism, local resonance, and frictional properties [34, 56].

2.4 Dynamical relations of MSL and tides

A tidal constituent amplitude can be expressed as a function of multiple variables:

$$Amp_{tidal} = f(H, r, \Psi_{\omega}, \dots) \quad (1)$$

Here, H is the water depth (which includes MSL, waves, storm surge, ocean stratification, river discharge, winds, etc.), r represents friction, and Ψ_{ω} is the frequency-dependent tidal response to astronomical tidal forcing. The “...” indicates other variabilities not considered here, e.g., wind. For a constituent amplitude to experience change (i.e., ΔAmp_{tidal}) it is necessary that one or more of these variables change, expressed by:

$$\Delta Amp_{tidal} = f(\Delta H, \Delta r, \Delta \Psi_{\omega}, \dots) \tag{2}$$

Subsequently, each of the variables that can change the tidal amplitudes depend on multiple factors:

$$\Psi_{\omega} = f(H, r, \dots) \rightarrow \Delta \Psi_{\omega} = f(\Delta H, \Delta r, \dots) \tag{3}$$

$$H = f(\rho, Q_r, \dots) \rightarrow \Delta H = f(\Delta \rho, \Delta Q_r, \dots) \tag{4}$$

$$r = f(H, \rho, \dots) \rightarrow \Delta r = f(\Delta H, \Delta \rho, \dots) \tag{5}$$

The depth-averaged tidal response function is therefore a function of astronomical forcing, water depth and the local frictional properties. Additionally, water depth may depend on vertical land movement [57], global sea-level rise [2], and other location-dependent environmental factors such as the local water density (ρ), local river discharge, Q_r [52], and local and far field wind forcing [21] effects. The effective frictional damping will be dependent on water depth, stratification, and mixing induced at the boundaries (bottom and surface). Finally, density ρ , as well as changes in buoyancy and stratification, are a function of water temperature, T_w , water salinity, T_s , river discharge, Q_r , and mixing, m_x :

$$\rho = f(T_w, S_w, Q_r, m_x, \dots) \rightarrow \Delta \rho = f(\Delta T_w, \Delta S_w, \Delta Q_r, \Delta m_x, \dots) \tag{6}$$

The chain rule can be applied to Eq. (2), and considering the possible changes of all factors yields a general expression for the variability in tidal amplitudes:

$$\Delta Amp_{tidal} = f(\Delta H, \Delta Q_r, \Delta \rho, \Delta m_x, \Delta r, \Delta \Psi_{\omega}, \dots) \tag{7}$$

It can be seen from this derivation that many of the variabilities can be correlated to each other. **Figure 1** shows a simple cartoon displaying the possible mechanisms that can affect MSL and tides, based on the derivations and references given above. Hence, the existence of multiple mechanisms, many of which may be

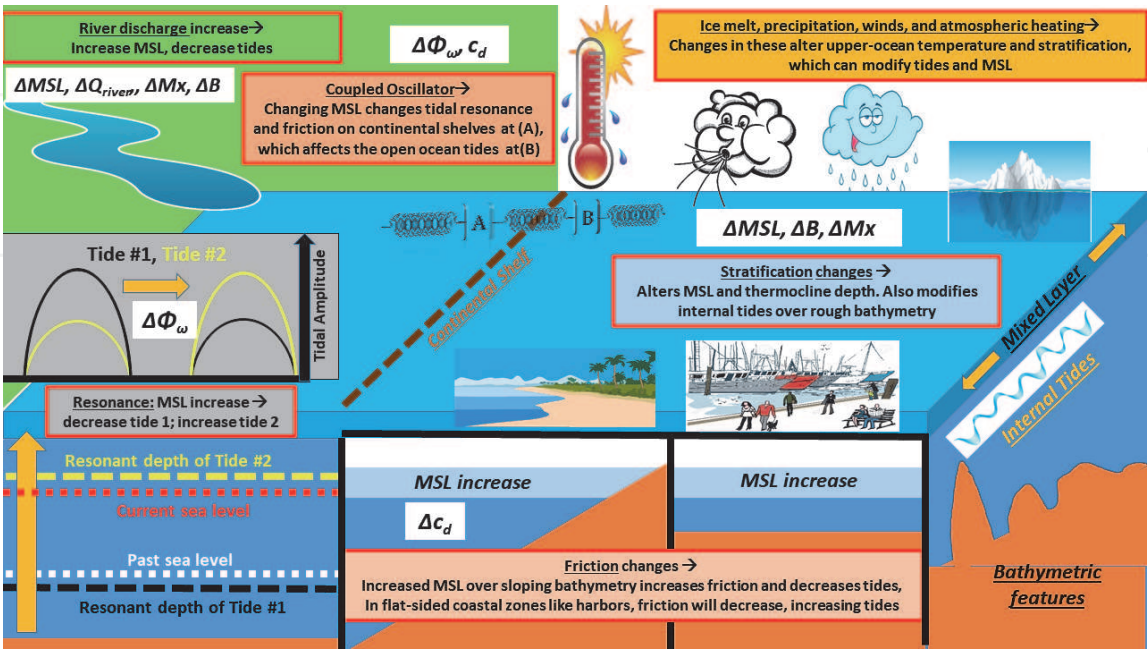


Figure 1. Schematic cartoon showing some of the mechanisms that can affect MSL and tides. See the text above for complete description of cartoon components.

correlated with each other, can make it difficult to discern the causes of observed variability. Yet, understanding these correlations is still vital, with the best strategy being to consider each location's dominating factors individually instead of relying on globally averaged solutions.

3. Methodology of tidal variability analysis

3.1 Tidal analysis

Recent studies have developed a reliable methodology to analyze tidal variability related to MSL variability [7–11]. These methods have been applied to many tide gauge locations worldwide, with a twofold approach. The first technique involves analyzing individual tidal constituents, while the second involves the consideration of the combination of multiple tides. For any individual tide gauge, water levels are typically recorded hourly as a continuous time series. Harmonic analysis of this data yields individual time series of multiple tidal constituents, each corresponding to an individual component of astronomical motion of the Sun and Moon, and their co-interactions. The largest parts of the tidal energy concentrate in the once-a-day (diurnal) and twice-a-day (semidiurnal) frequency bands, with several closely spaced tidal constituents being important in each band. In practice, however, only a small number of these contain most of the tidal energy. For the purposes of our discussions of past studies we will only need to mention a few. The major twice-daily (semidiurnal) tide due to the Moon is denoted M_2 , and the twice-daily tide due to the Sun is denoted S_2 . Two important lunisolar interaction tides that define the once-a-day (diurnal) tides are denoted K_1 and O_1 . Most of the past analyses only consider these four components, however, some of the locations considered (in the Atlantic Ocean) also consider two more semidiurnal components, denoted N_2 and K_2 , and two more diurnal components, P_1 and Q_1 (Table 1).

3.2 Tidal admittance calculations

Investigations of tidal trends are carried out using a tidal admittance method. An admittance is the unit-less ratio of an observed tidal constituent to the corresponding tidal constituent in the astronomical tide generating force (ATGF) expressed as a potential, V , divided by the acceleration due to gravity, g , to yield a quantity, $Z_{pot}(t) = V/g$, with units of length that can be compared to tidal elevations $Z_{obs}(t)$ on a constituent by constituent basis. Because nodal and other low-frequency astronomical variability is present with similar strength in both the observed tidal record and in V , its effects are eliminated in the yearly analyzed admittance time series. Yearly tidal harmonic analyses are performed at monthly time steps on both the observed tidal records and the hourly $Z_{pot}(t)$ at the same location, using the *r_t_tide* MATLAB package [58], a robust analysis suite based on *t_tide* [59]. The tidal potential is determined based on the methods of Cartwright and Tayler [24], and Cartwright and Edden [60]. The result from a single harmonic analysis of $Z_{obs}(t)$ or $Z_{pot}(t)$ determines an amplitude, A , and phase, θ , at the central time of the analysis window for each tidal constituent, with error estimates. Analyzing the entire tide gauge record produces time-series of amplitude and phase. From amplitude $A(t)$ and phase $\theta(t)$ time series, one can construct complex amplitudes $Z(t)$:

$$Z(t) = A(t)e^{i\theta(t)} \quad (8)$$

Station name	Country	Lat.(N)	Long. (E)	K ₁	(±)	M ₂	(±)	δ-HAT	(±)
Northeast Pac.									
French Frigate Sh.	USA	23.87	−166.28	−8.52	4.44	−33.37	9.36	−52.62	16.89
Cabo San Lucas	Mexico	22.88	−109.92	−8.83	3.06	39.78	12.45	57.75	64.52
Kodiak Island, Alaska	USA	57.73	−152.52	12.96	10.03	20.84	7.79	12.27	18.80
Adak, Alaska	USA	51.87	−176.63	47.76	15.62	−11.11	7.46	11.60	17.66
Dutch Harbor, Alaska	USA	53.88	−166.53	−44.37	14.73	−2.59	8.26	−61.00	17.63
Midway	USA	28.22	−177.37	−2.07	5.62	6.03	8.61	−15.74	15.04
Johnston	USA	16.75	−169.52	−32.27	11.78	−29.85	16.25	−116.88	24.45
Honolulu, Hawaii	USA	21.3	−157.87	−9.03	6.53	140.77	23.35	139.51	21.62
Nawiliwili Bay, Hawaii	USA	21.97	−159.35	−3.63	5.87	61.28	13.80	55.61	12.27
Kahului, Hawaii	USA	20.9	−156.47	2.60	7.52	−43.41	8.79	−13.41	7.19
Hilo, Hawaii	USA	19.73	−155.07	12.90	5.96	131.07	14.35	146.75	12.18
Mokuoloe, Hawaii	USA	21.43	−157.8	38.77	6.45	6.35	14.28	44.24	25.30
Tofino	Canada	49.15	−125.92	6.25	8.01	44.64	8.41	13.39	31.77
Victoria	Canada	48.42	−123.37	−1.66	17.45	−33.09	12.66	−60.30	43.39
San Francisco, California	USA	37.8	−122.47	−70.20	10.99	−80.34	21.57	−146.56	35.20
La Jolla, California	USA	32.87	−117.25	16.03	12.40	28.83	12.57	59.50	34.60
Monterey, California	USA	36.6	−121.88	1.40	10.29	31.79	5.07	27.37	22.30
Crescent City, California	USA	41.75	−124.18	−15.27	10.44	−9.50	11.40	−48.44	12.73
Neah Bay, Washington	USA	48.37	−124.62	4.50	8.21	−11.95	6.26	9.80	14.06
Sitka, Alaska	USA	57.05	−135.35	−20.61	12.37	21.93	15.29	−23.03	39.63
Seward, Alaska	USA	60.12	−149.43	3.27	11.30	5.68	11.70	−8.19	25.83
Seldovia, Alaska	USA	59.43	−151.72	21.69	17.88	−63.71	25.41	−53.76	40.79

Station name	Country	Lat.(N)	Long. (E)	K ₁	(±)	M ₂	(±)	δ-HAT	(±)
Valdez, Alaska	USA	61.13	−146.37	17.86	19.01	12.24	16.33	52.06	18.79
Port San Luis, California	USA	35.18	−120.77	−10.55	12.57	12.68	6.89	4.49	18.17
Los Angeles, California	USA	33.72	−118.27	−11.03	10.87	−7.38	7.33	−21.39	17.05
San Diego, California	USA	32.72	−117.17	−13.71	7.29	−0.87	7.02	−17.77	17.18
Yakutat, Alaska	USA	59.55	−139.73	−7.87	11.12	2.48	13.54	21.99	41.13
Ketchikan, Alaska	USA	55.33	−131.63	−1.48	11.66	10.32	12.64	21.89	15.73
Astoria, Oregon	USA	46.22	−123.77	−32.65	10.87	−91.81	16.36	−256.81	35.09
Charleston, Oregon	USA	43.35	−124.32	0.64	7.90	−0.08	8.72	−17.47	18.59
Santa Monica, California	USA	34.02	−118.5	−2.46	12.81	−38.31	6.77	−51.72	47.75
Cordova, Alaska	USA	60.57	−145.75	31.25	15.59	10.45	16.29	16.24	14.86
South Beach, Oregon	USA	44.63	−124.05	−18.06	9.08	5.08	8.58	−16.05	40.56
Seattle, Washington	USA	47.6	−122.4	14.68	14.84	−13.26	10.09	−34.64	37.09
Vancouver	Canada	49.29	−123.11	−33.85	32.52	−42.29	32.99	−160.29	53.48
Point Atkinson	Canada	49.34	−123.25	−41.09	44.91	−30.66	44.21	−97.58	232.94
Bella Bella	Canada	52.16	−128.14	−33.68	10.94	15.34	13.91	−35.24	33.36
Queen Charlotte	Canada	53.25	−132.07	7.91	15.64	47.42	49.37	1.47	71.85
Port Hardy	Canada	50.72	−127.49	−33.95	14.16	8.94	23.59	−12.79	36.92
Bamfield	Canada	48.84	−125.14	−7.67	9.78	−3.59	13.20	11.02	26.28
Southeast Pac.									
Baltra	Ecuador	−0.43	−90.28	7.28	4.66	27.08	5.22	26.89	18.15
Papeete (Tahiti)	Fr. Poly.	−17.53	−149.57	−10.12	7.75	−136.07	33.43	−95.29	43.32
Juan Fern Island	Chile	−33.62	−78.83	−4.57	6.50	−16.53	4.92	−28.68	11.47
Easter Island	Chile	−27.15	−109.45	−3.57	6.44	−7.74	8.94	28.73	24.75

Station name	Country	Lat.(N)	Long. (E)	K ₁	(±)	M ₂	(±)	δ-HAT	(±)
Rarotonga	Cook Is.	−21.2	−159.78	10.79	3.36	16.68	12.11	49.97	20.53
Penrhyn	Cook Is.	−8.98	−158.05	17.77	3.59	27.57	6.00	31.33	18.75
Santa Cruz	Ecuador	−0.75	−90.32	3.16	2.52	−22.93	11.02	−34.78	25.26
San Felix	Chile	−26.28	−80.13	14.34	4.05	45.31	11.31	79.63	36.25
Nuku'alofa	Tonga	−21.13	−175.17	5.44	4.11	−42.04	10.64	−103.31	10.30
Antofagasta	Chile	−23.65	−70.4	−6.79	6.72	1.77	10.92	−33.28	5.49
Valparaiso	Chile	−33.03	−71.63	11.31	10.34	−2.27	22.44	−122.85	38.33
Lobos de Afuera	Peru	−6.93	−80.72	3.46	4.21	38.64	10.79	23.92	16.59
Buena Ventura	Colombia	3.9	−77.1	−14.51	4.14	−8.24	31.63	−81.61	16.93
Caldera	Chile	−27.07	−70.83	40.34	6.74	51.24	10.74	127.40	27.28
La Libertad	Ecuador	−2.2	−80.92	−6.04	3.86	−72.17	19.85	−73.11	16.75
Matarani	Peru	−17	−72.12	−18.57	4.27	−20.16	9.34	−40.29	22.12
Balboa	Panama	8.97	−79.57	−1.38	2.67	−27.46	8.98	−56.77	11.19
Tumaco	Colombia	1.83	−78.73	−3.10	3.14	9.79	19.83	33.97	21.07
Puerto Montt	Chile	−41.48	−72.97	−81.37	16.93	−610.13	99.43	−963.21	107.66
Northwest Pac.									
Chichijima	Japan	27.1	142.18	12.13	10.78	−11.32	13.99	−17.09	20.63
Hong Kong	China	22.3	114.22	308.37	42.97	292.49	50.31	665.44	99.23
Kaohsiung	Taiwan	22.62	120.28	17.19	5.11	−4.74	8.47	−17.48	16.91
Keelung	Taiwan	25.15	121.75	−25.79	8.79	−48.15	13.64	−54.28	53.95
Nakanoshima	Japan	29.83	129.85	−15.68	13.07	53.18	29.44	47.39	36.07
Abashiri	Japan	44.02	144.28	−52.16	17.57	−30.74	6.12	−126.15	47.40
Hamada	Japan	34.9	132.07	45.18	19.21	−26.27	7.07	56.95	83.61

Station name	Country	Lat.(N)	Long. (E)	K ₁	(±)	M ₂	(±)	δ-HAT	(±)
Toyama	Japan	36.77	137.22	−27.94	14.91	−0.49	6.12	−29.18	37.40
Kushiro	Japan	42.97	144.38	53.69	11.20	−17.03	8.16	−43.71	22.09
Ofunato	Japan	39.07	141.72	13.39	11.44	−34.36	8.83	−78.73	32.98
Mera	Japan	34.92	139.83	−79.54	16.67	17.51	14.68	−100.04	9.57
Kushimoto	Japan	33.47	135.78	16.35	9.90	17.82	25.25	−25.03	26.31
Aburatsu	Japan	31.57	131.42	38.75	10.78	−11.91	15.38	36.18	12.17
Naha	Japan	26.22	127.67	3.88	8.08	1.31	12.50	39.46	18.16
Maisaka	Japan	34.68	137.62	−71.20	12.49	−100.99	18.78	−350.29	29.25
Miyakejima	Japan	34.07	139.48	−12.04	4.10	−17.33	3.84	−55.27	8.44
Naze	Japan	28.38	129.5	−11.61	7.86	−44.00	11.37	−29.62	29.23
Wakkanai	Japan	45.4	141.68	−30.41	18.19	7.10	10.61	−108.48	22.70
Nagasaki	Japan	32.73	129.87	−18.21	9.60	−84.81	22.61	−85.53	28.09
Nishinoomote	Japan	30.73	131	5.24	8.35	4.67	14.57	14.34	34.65
Hakodate	Japan	41.78	140.73	8.66	14.45	7.66	10.04	11.96	24.16
Ishigaki	Japan	24.33	124.15	27.59	10.49	−101.09	13.26	−85.53	17.11
Hachinohe	Japan	40.53	141.53	−21.13	9.67	−20.69	7.18	−82.28	23.08
Hanasaki	Japan	48.28	145.58	4.92	4.87	−9.99	5.93	53.59	17.67
Kamaishi	Japan	39.27	141.89	20.34	11.48	−9.73	15.15	−13.60	49.69
Minamizu	Japan	34.63	138.89	−3.59	8.10	18.81	9.24	−15.73	23.52
Miyako	Japan	39.63	141.97	3.63	8.02	−34.28	10.34	−18.20	9.85
Nagoya	Japan	35.08	136.88	−17.08	6.58	29.19	8.22	2.49	7.05
Omaezaki	Japan	34.6	138.23	9.08	7.29	−35.90	6.80	−29.21	38.98
Onahama	Japan	36.93	140.92	24.81	11.15	−30.12	11.23	−42.33	31.63

Station name	Country	Lat.(N)	Long. (E)	K ₁	(±)	M ₂	(±)	δ-HAT	(±)
Owase	Japan	34.07	136.22	0.61	6.40	15.47	4.84	−3.58	12.84
Toba	Japan	34.47	136.85	−9.90	7.91	13.56	25.85	−85.16	14.55
Tokyo	Japan	35.67	139.77	−52.32	7.96	−32.71	15.18	−137.30	31.50
Urigami	Japan	33.55	135.9	−18.83	6.86	−35.15	13.16	32.69	18.72
Odomari	Japan	31.02	130.69	−9.46	8.14	−101.22	14.67	−193.72	52.20
Okada	Japan	34.78	139.4	20.32	8.69	78.65	15.14	158.85	20.41
Shimizuminato	Japan	35.02	138.5	−50.66	12.38	−57.18	14.54	−208.53	54.03
Shirihama	Japan	33.68	135.38	13.51	6.39	−47.26	13.33	−38.17	34.38
Tosashimizu	Japan	32.78	132.97	1.62	7.79	1.10	8.35	−81.37	56.50
Southwest Pac.									
Pohnpei	Micronesia	6.98	158.25	21.28	5.37	9.68	15.66	−6.22	14.96
Nauru	Rep of Nauru	−0.53	166.92	−2.33	6.78	−20.22	9.46	−53.89	7.83
Majuro	Rep Marshall Is	7.12	171.37	0.77	7.57	−2.52	16.65	−26.84	20.39
Malakal	Rep of Belau	7.33	134.47	50.30	5.19	−27.23	7.01	4.34	24.61
Yap	Fd St Micronesia	9.52	138.13	24.44	6.77	−39.92	7.01	−57.78	25.15
Honiara	Solomon Islands	−9.42	159.95	4.00	4.23	64.61	4.71	66.79	10.13
Rabaul	Pap. New Guinea	−4.2	152.18	−30.61	3.82	103.43	9.22	30.36	7.86
Christmas Island	Rep of Kiribati	1.98	−157.47	−7.59	3.68	−50.00	8.77	−70.51	8.38
Suva	Fiji	−18.13	178.43	−2.86	4.92	59.61	16.99	71.90	68.46
Noumea	France	−22.3	166.43	27.01	10.82	21.36	38.45	73.12	28.04
Funafuti	Fiji	−8.5	179.22	−8.33	4.16	−27.28	8.38	−26.57	30.14
Saipan	N. Mari. Islands	15.23	145.75	7.19	12.54	34.13	17.96	−5.84	14.93
Kapingamarangi	Fd St Micronesia	1.1	154.78	−21.95	6.02	36.75	8.44	15.71	15.00

Station name	Country	Lat.(N)	Long. (E)	K ₁	(±)	M ₂	(±)	δ-HAT	(±)
Port Villa	Vanuatu	−17.77	168.3	−11.72	4.86	82.47	19.47	74.19	52.38
Wake	USA	19.28	166.62	2.14	7.14	62.21	24.97	−24.16	31.65
Guam	Guam	13.43	144.65	−26.24	12.26	−8.45	17.93	−115.92	17.85
Kwajalein	Marshall Islands	8.73	167.73	1.07	5.62	12.76	12.49	38.25	12.64
Pago Pago	USA	−14.28	−170.68	14.34	3.64	21.05	17.03	28.16	21.31
Manus Island	Pap. New Guinea	−2.02	147.27	−15.77	10.06	−26.10	13.99	0.36	51.64
Wellington	New Zealand	−41.28	174.78	−7.37	7.82	−17.48	19.95	−39.35	17.88
Cendering	Malaysia	5.27	103.18	−4.83	16.88	−57.34	10.35	−131.72	67.22
Johor Bahru	Malaysia	1.47	103.8	−109.04	28.62	−175.99	27.86	−232.08	36.09
Kuantan	Malaysia	3.98	103.43	−57.48	18.26	−67.71	21.92	−216.82	53.51
Tioman	Malaysia	2.8	104.13	−79.55	20.41	−87.70	27.24	−292.35	48.19
Sedili	Malaysia	1.93	104.12	−118.19	21.58	−74.64	28.15	−215.36	107.81
Kukup	Malaysia	1.33	103.45	−17.17	14.89	−97.15	15.16	−184.56	59.35
Getting	Malaysia	6.23	102.1	−23.03	9.98	−44.19	10.05	−83.72	103.62
Ko Lak	Thailand	11.8	99.82	30.32	26.28	29.16	7.93	−42.28	53.26
Tanjong Pagar	Singapore	1.27	103.85	−140.02	31.09	0.18	32.51	4.46	9.54
Kelang	Malaysia	3.05	101.37	12.01	14.74	−152.54	14.72	−152.29	34.13
Kaling	Malaysia	2.22	102.15	−78.24	14.28	−83.51	9.09	−218.47	57.52
Langkawi	Malaysia	6.43	99.75	−14.33	5.61	−83.03	12.81	−143.79	37.15
Lumut	Malaysia	4.23	100.62	−2.44	12.17	−76.20	7.31	−116.95	42.95
Penang	Malaysia	5.42	100.35	−4.51	7.46	−95.06	11.40	−138.73	29.69
Ko Taphao Noi	Thailand	7.83	98.43	−2.85	4.33	−62.23	14.66	−70.35	32.54
Vung Tau	Vietnam	10.33	107.07	59.30	16.80	−1.71	37.52	108.00	87.06

Station name	Country	Lat.(N)	Long. (E)	K_1	(\pm)	M_2	(\pm)	δ -HAT	(\pm)
Kota Kinabalu	Malaysia	5.98	116.07	-1.72	11.41	-21.09	5.90	-67.18	23.90
Bintulu	Malaysia	3.22	113.07	287.13	44.81	-23.43	13.76	614.89	140.46
Sandakan	Malaysia	5.82	118.07	49.54	10.99	24.79	9.18	107.56	28.17
Brisbane	Australia	-27.37	153.17	0.40	17.56	-6.46	48.04	272.56	39.62
Bundaberg	Australia	-24.83	152.35	5.54	5.40	-18.03	7.09	-13.85	19.94
Ft. Denison	Australia	-33.85	151.23	-0.92	0.28	-13.98	0.35	-2.46	20.72
Townsville	Australia	-19.25	146.83	-1.52	5.17	6.23	12.47	-11.58	12.32
Spring Bay	Australia	-42.55	147.93	19.69	12.34	-81.68	29.84	-87.50	80.18
Booby Island	Australia	-10.6	141.92	25.44	24.63	-6.48	15.22	19.60	79.56
Hobart	Australia	-42.88	147.33	-20.13	11.19	19.65	15.83	27.53	23.14
Manila	Philippines	14.58	120.97	33.98	25.32	-92.68	14.56	-118.76	66.57
Legaspi	Philippines	13.15	123.75	-21.13	7.33	-146.09	21.30	-144.79	36.48
Davao	Philippines	7.08	125.63	191.90	22.16	-79.66	14.90	68.99	89.72
Lord Howe Island	Australia	-31.52	159.07	4.80	7.23	-7.22	12.74	10.24	27.38
Lautoka	Fiji	-17.6	177.43	4.14	3.07	23.39	10.60	53.80	19.66
Cairns	Australia	-16.92	145.77	-1089.03	477.48	109.08	20.28	297.56	1274.52
Gladstone	Australia	-23.85	151.26	-146.62	515.09	36.50	39.90	-40.45	300.49
Williamstown	Australia	-37.86	144.89	398.57	186.07	9.63	15.64	145.75	568.48

All values are expressed as millimeter change in tide per meter rise in MSL (mm m^{-1}).
Significant values are in bold text, based on a SNR > 2, and an absolute magnitude of $>10 \text{ mm m}^{-1}$.

Table 1.
Tidal anomaly correlations (TACs) in the Pacific for M_2 , K_1 and δ -HAT, along with 95% confidence limits.

Time-series of tidal admittance amplitude (**A**) and phase lag (**P**) for a constituent are formed using Eqs. (9) and (10):

$$\mathbf{A}(t) = \text{abs} \left| \frac{Z_{\text{obs}}(t)}{Z_{\text{pot}}(t)} \right| \quad (9)$$

$$\mathbf{P}(t) = \theta_{\text{obs}}(t) - \theta_{\text{pot}}(t) \quad (10)$$

The harmonic analysis that generates the **As** and **Ps** also provides an MSL time-series. For each resultant dataset (MSL, **A** and **P**), the mean and trend are removed from the time series, to allow direct comparison of their co-variability around the trend. Applying trend removal also reduces the effects of land motions (e.g., glacial isostatic adjustment (GIA), subsidence, and tectonic effects. All of these are assumed linear on the time scale of tidal records) that occur on longer time scales, whereas we are concerned with short-term variability.

3.3 Tidal anomaly correlations (TAC)

Tidal range changes are quantified using tidal anomaly correlations (TACs), the relationships of detrended short-term tidal variability to detrended short-term MSL fluctuations. These are used to determine the sensitivity of individual constituents to a sea-level perturbation, and the result is expressed as a millimeter change in constituent amplitude per meter change in sea-level. The M_2 , S_2 , K_1 , and O_1 tidal constituents are first considered separately, and later in combination as a proxy for the change in the highest astronomical tide (δ -HAT). We assume that the interannual variability captured by TACs can be extrapolated to the longer time scales, subject to the qualification that the changes remain “small-amplitude”, meaning a 0.5–1 m change in MSL and a change in tidal amplitude of a few tens of cm. Thus, we report TACs in units of mm m^{-1} . The detrended time series of **A** and **P** can each be compared to detrended MSL, but herein, only the absolute magnitudes of the **A** for major constituents will be considered, because of their direct role in changing high water levels. The slope of the regression between **A** and MSL is the definition of the TA, deemed significant if the signal to noise ratio (found from comparing the magnitude of the TAC to the 95% confidence interval (CI) of the robust fitting error) is greater than 2.0.

3.4 Example of a TAC

The M_2 TAC results at Honiara in the Solomon Islands exhibits one of the clearest signals in our data inventory. **Figure 2** shows the M_2 TAC at Honiara on the island of Guadalcanal (Solomon Islands, 9.4167°S and 159.950°E). The M_2 tide amplitude is relatively small at this location (~ 50 mm), but the anomaly correlation is large, $+58.9 \pm 3.7 \text{ mm m}^{-1}$ (118% of the local M_2 amplitude), and very coherent. Since the trend is reasonably linear over such a large range ($>100\%$ in terms of tidal amplitude and ~ 0.45 m MSL), our analysis approach is demonstrated to be valid, even in cases where the small amplitude assumption is stretched.

3.5 Change in the highest astronomical tide (δ -HAT)

We also consider a combined tidal variability besides the individual TACs. The M_2 , S_2 , K_1 , and O_1 variabilities are summed to produce a combined tidal variability that is compared to MSL (δ -HAT). The δ -HAT is a proxy for the change in the highest astronomical tide, which is estimated by combining the complex time series

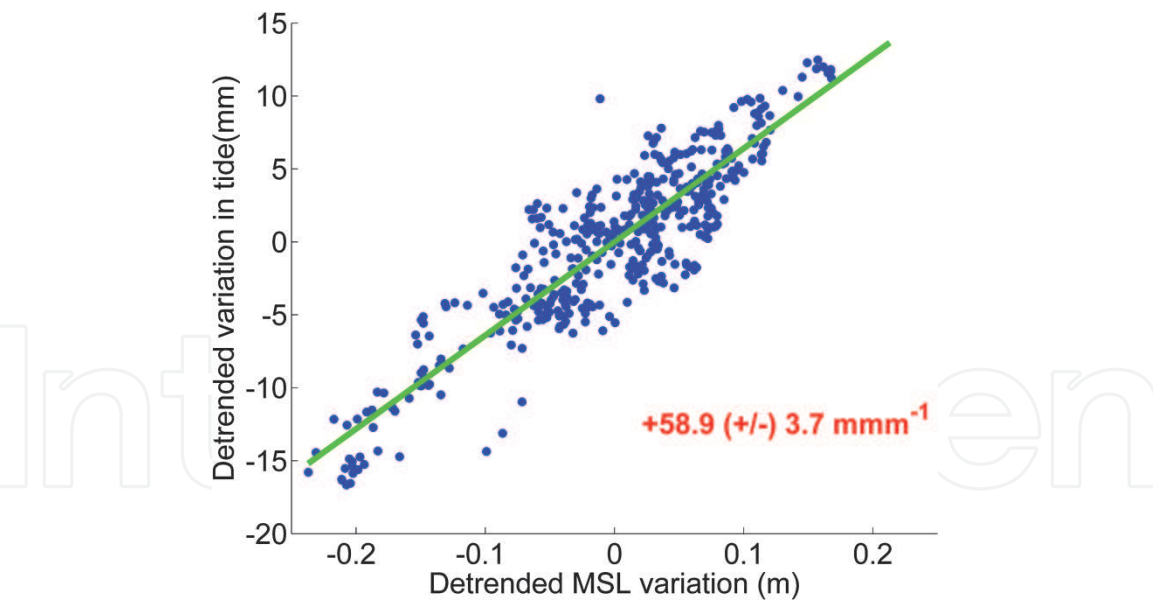


Figure 2.
M₂ TAC relation of detrended absolute tidal amplitude to detrended MSL at Honiara in the Solomon Islands [9]. The green line is a robust linear regression trend, in mmm^{-1} .

of the yearly analyzed M_2 , S_2 , K_1 , and O_1 tides, approximately 75% of the full tidal height. “Complex” means, in this context, that each constituent is considered as a complex number (accounting for both amplitude and phase), the complex vectors are added, and the total amplitude is resolved from the complex sum. The detrended time series of δ -HAT is then compared to the detrended MSL variability. The magnitude of the slope of the regression is the definition of the δ -HAT, and, like the TACs, we report δ -HATs in units of mm m^{-1} . Theoretically, the four constituents will not be exactly in phase more than once during every 18.6-year nodal cycle, though the constituents may be approximately aligned more often; therefore, this summation provides a suitable proxy for the envelope of possible tidal amplitudes. A detailed description of the step-by-step method, with additional figures showing the intermediate steps in the process, are provided in the supplementary materials of Devlin et al. [8]. The δ -HAT analyses performed for the Atlantic tide gauge stations [10] employed an eight-tide combination, which adds the N_2 , K_2 , P_1 and Q_1 tidal constituents to the δ -HAT sum (Table 2).

3.6 Error analysis and autocorrelation handling

Our approach uses one-year harmonic analyses at a one-month step to yield smooth time-series. However, this approach must be taken with caution, as there may be autocorrelation in the regression due to data overlap. Thus, calculations of regressions and associated statistics (i.e., the p -values) are based on a sub-sampled dataset of one determination per year. The definition of the “year window” used for harmonic analysis may influence the value of the TAC or δ -HAT, i.e. calendar year (Jan–Dec) vs. water year (Oct–Sep). Thus, we use an ensemble of TACs and δ -HATs using 12 distinct year definitions (i.e., Jan–Dec, Feb–Jan, ...). We take the average of this set as the magnitude of the TAC or δ -HAT. For an estimate of the confidence interval of the trend, the interquartile range (middle 50% of the set range) is used. We consider correlations to be significant if they have a p -level of <0.05 , the trend is greater than the interquartile range by at least a factor of 1.5, and the magnitude is greater than $\pm 10 \text{ mm m}^{-1}$ for individual TACs, and greater than $\pm 50 \text{ mm m}^{-1}$ for the δ -HATs. Some determinations had unexpected errors or grossly insignificant statistics (especially for the shorter records) that made them

Station	Country	Lat (N)	Long(E)	M ₂ TAC	IQR	K ₁ TAC	IQR	δ-HAT	IQR
Charlotte Amalie	USA	18.34	−64.92	25.7	2.9	9.2	5.5	15.0	7.8
Magueyes Island	USA	17.97	−67.05	−10.3	8.6	14.5	8.0	−56.0	7.9
San Juan	USA	18.47	−66.12	35.7	2.7	39.6	13.8	177.7	23.8
Cristobal	Panama	9.36	−79.92	−27.1	6.2	6.7	5.8	−1.9	13.7
Cartagena	Columbia	10.38	−75.53	−1.8	8.9	27.7	18.8	−19.5	41.3
Port Isabel, Texas	USA	26.06	−97.22	−8.6	1.9	1.6	10.0	−31.1	27.6
Corpus Christi, Texas	USA	27.58	−97.22	3.1	3.4	4.9	8.8	14.5	24.0
Rockport, Texas	USA	28.02	−97.05	−3.8	1.9	0.5	6.5	−0.2	11.1
Freeport, Texas	USA	28.95	−95.31	−12.6	7.2	10.4	22.5	−17.8	35.9
Galveston Pl. Pier, Texas	USA	29.29	−94.79	−0.1	6.6	7.9	16.9	−5.7	48.3
Galveston Pier 21, Texas	USA	29.31	−94.79	−57.6	8.6	9.0	13.7	−116.4	49.5
Sabine Pass N, Texas	USA	29.73	−93.87	−25.1	8.9	−1.0	12.9	−49.9	37.2
Grand Isle, Louisiana	USA	29.26	−89.96	0.1	3.8	25.8	6.4	39.4	9.3
Dauphin Island, Alabama	USA	30.25	−88.08	−1.6	18.1	33.3	21.8	47.8	50.8
Pensacola, Florida	USA	30.40	−87.21	9.0	4.7	32.0	12.2	112.5	24.3
Panama City Beach, Florida	USA	30.21	−85.88	12.2	2.8	0.8	22.7	109.5	59.7
Apalachicola, Florida	USA	29.73	−84.98	12.7	6.0	−53.9	19.7	−74.5	33.1
Saint Petersburg, Florida	USA	27.76	−82.63	102.4	23.3	36.3	21.5	296.5	70.6
Naples, Florida	USA	26.13	−81.81	49.3	29.3	−14.2	16.2	139.0	53.2
Key West, Florida	USA	24.55	−81.81	−4.9	9.9	−1.1	14.3	−6.9	39.1
Settlement Point	Bahamas	26.72	−78.98	189.6	30.8	−5.4	5.4	323.1	33.7
Virginia Key, Florida	USA	25.73	−80.16	21.4	5.8	−42.1	17.4	−48.3	29.4
Port Canaveral, Florida	USA	28.42	−80.59	−15.0	23.0	−10.7	9.9	−56.8	41.8
Fernandina Beach, Florida	USA	30.67	−81.47	−54.7	5.9	4.6	10.6	−91.6	9.2
Fort Pulaski, Georgia	USA	32.03	−80.90	−87.9	14.0	−10.4	8.0	−132.5	61.0
Charleston, S. Carolina	USA	32.78	−79.93	−107.6	5.6	−11.7	6.0	−157.7	30.3
Springmaid, S. Carolina	USA	33.66	−78.92	−42.0	20.3	27.5	3.5	4.5	10.7
Wilmington, N. Carolina	USA	34.23	−77.59	−211.4	60.5	−38.0	12.1	−413.3	141.2
Duck Pier, N. Carolina	USA	35.18	−75.75	−12.6	3.5	−18.9	6.3	−13.4	39.5
Sewells Point, Virginia	USA	36.95	−76.33	−21.7	1.6	−30.2	6.2	−50.6	29.2
Chesapeake BBT, Virginia	USA	36.97	−76.11	−10.1	5.7	−33.5	8.2	−39.0	18.0
Kiptopeke, Virginia	USA	37.17	−75.99	55.8	7.5	−32.2	11.9	86.0	25.7
Cambridge II, Maryland	USA	38.57	−76.07	31.1	9.7	−2.9	26.7	70.6	55.7

Station	Country	Lat (N)	Long(E)	M ₂ TAC	IQR	K ₁ TAC	IQR	δ-HAT	IQR
Washington, DC	USA	38.87	−77.02	−78.4	25.0	−16.4	8.6	−91.8	42.8
Annapolis, Maryland	USA	38.98	−76.48	2.3	17.4	−27.0	9.9	6.0	45.8
Baltimore, Maryland	USA	39.27	−76.58	35.2	5.6	−25.5	16.1	68.7	36.5
Lewes, Delaware	USA	38.78	−75.12	3.4	10.9	−2.6	7.0	79.7	29.6
Cape May, New Jersey	USA	38.97	−74.96	19.9	29.1	1.6	13.9	104.3	15.1
Reedy Point, Maryland	USA	39.56	−75.57	97.6	48.4	−3.9	17.1	142.8	62.2
Philadelphia, Pennsylvania	USA	39.93	−75.14	17.5	24.5	−6.5	10.1	72.6	41.5
Atlantic City, New Jersey	USA	39.36	−74.42	−20.5	6.0	−6.0	18.5	−59.7	21.3
Sandy Hook, New Jersey	USA	40.47	−74.01	23.4	13.7	−36.0	7.5	54.1	35.1
New York City, New York	USA	40.70	−74.01	50.3	26.0	−0.8	18.7	57.3	36.2
Montauk, New York	USA	41.05	−71.96	4.9	6.1	−14.6	15.4	13.8	16.4
Bridgeport, Connecticut	USA	41.17	−73.18	−39.7	20.1	−43.7	9.6	−10.2	53.0
New London, Connecticut	USA	41.36	−72.09	15.0	3.2	−23.3	12.1	14.5	22.5
Newport, Rhode Island	USA	41.51	−71.33	−0.1	9.5	−13.0	22.9	33.2	31.7
Providence, Rhode Island	USA	41.81	−71.40	−4.7	8.1	−4.6	13.4	2.5	21.4
Nantucket, Massachusetts	USA	41.29	−70.10	8.0	13.1	−2.3	4.6	130.7	17.0
Woods Hole, Massachusetts	USA	41.52	−70.67	38.6	7.6	−7.3	8.8	69.2	34.4
Boston, Massachusetts	USA	42.36	−71.05	−48.8	14.9	−18.2	5.8	86.6	28.6
Portland, Maine	USA	43.66	−70.25	−79.6	43.6	−30.0	11.0	−3.9	50.9
Bar Harbor, Maine	USA	44.39	−68.21	62.4	16.0	0.9	12.4	243.0	63.2
Eastport, Maine	USA	44.90	−66.98	−145.8	16.7	−23.1	8.2	27.2	46.9
Saint John	Canada	45.25	−66.06	−258.7	35.2	−2.0	5.5	−378.0	39.0
Yarmouth	Canada	43.83	−66.12	−7.0	56.5	−11.0	11.8	55.2	96.6
Halifax	Canada	44.67	−63.58	25.1	27.7	−11.3	8.3	71.6	12.0
Charlottetown	Canada	46.23	−63.12	53.3	12.6	−71.0	16.1	−47.4	20.3
North Sydney	Canada	46.22	−60.25	−3.6	7.3	−30.1	17.4	26.3	48.6
Lower Escuminac	Canada	47.08	−64.88	−18.7	10.9	−77.8	27.2	−94.1	18.6
Port-aux-Basques	Canada	47.57	−59.13	−23.9	6.7	−19.8	7.2	−92.8	29.9
Argentua	Canada	47.30	−53.98	−15.9	13.2	−54.2	3.6	−19.5	8.6
St. Johns	Canada	47.57	−52.72	−3.5	3.3	−5.2	3.8	−26.5	19.6
Churchill	Canada	58.78	−94.20	16.3	100.7	7.5	8.1	51.3	272.4
Reykjavik	Iceland	64.15	−21.94	−14.9	17.8	0.8	8.2	−118.2	43.6
Ny-Aelsund	Norway	78.93	11.95	−10.4	3.0	−5.5	3.7	64.5	29.6

Station	Country	Lat (N)	Long(E)	M ₂ TAC	IQR	K ₁ TAC	IQR	δ-HAT	IQR
Vardo	Norway	70.33	31.10	−0.7	13.7	5.0	8.1	−3.2	25.7
Honningsvaag	Norway	70.98	25.97	−20.2	13.2	−10.9	13.1	−108.3	44.9
Andenes	Norway	69.32	16.15	−8.4	5.5	−1.4	12.7	−14.1	13.5
Rorvik	Norway	64.87	11.25	−23.2	5.7	−16.2	7.9	−60.5	23.2
Heimsjoe	Norway	63.43	9.10	−20.2	5.8	−12.4	7.5	−82.2	27.0
Maaloey	Norway	61.93	5.11	1.3	17.1	4.7	9.8	−21.1	48.0
Wick	UK	58.44	−3.09	8.7	11.8	15.0	8.5	47.0	86.8
Kinlochbervie	UK	58.46	−5.05	−14.3	6.3	−6.2	7.3	−105.8	64.4
Stornoway	UK	58.21	−6.39	−43.4	19.5	5.7	12.1	−110.8	51.6
Aberdeen	UK	57.14	−2.07	−8.6	4.1	−5.3	3.2	−43.3	41.8
Leith (Edinburgh)	UK	55.99	−3.18	−46.2	35.0	28.5	33.5	−48.2	147.7
North Shields	UK	55.01	−1.44	2.9	10.5	−2.3	7.4	166.7	43.6
Whitby	UK	54.49	−0.61	10.3	17.0	−59.2	27.8	32.9	128.3
Immingham	UK	53.63	−0.19	48.0	26.5	2.9	7.8	84.4	69.7
Cromer	UK	52.94	1.30	29.2	9.3	−7.8	7.0	148.0	18.8
Lowestoft	UK	52.47	1.75	46.4	27.8	12.9	28.0	293.6	69.1
Felixstowe	UK	51.96	1.35	−80.0	54.9	−28.1	12.0	−203.4	55.1
Sheerness	UK	51.44	0.74	−46.3	83.9	−11.7	2.6	−109.9	20.5
Dover	UK	51.12	1.32	−135.7	80.4	18.0	7.5	−276.5	87.2
Newhaven	UK	50.78	0.06	−100.5	28.9	−21.5	12.1	−212.6	69.0
Portsmouth	UK	50.80	−1.11	−23.2	5.5	−4.4	6.7	−157.5	65.7
Bournemouth	UK	50.71	−1.87	−2.0	40.9	33.1	12.5	−8.4	132.0
Weymouth	UK	50.61	−2.45	−57.5	17.4	−1.8	11.1	−42.7	59.7
Devonport	UK	50.37	−4.19	−38.4	20.6	30.5	16.2	−48.7	170.3
Newlyn	UK	50.10	−5.52	−52.7	23.7	17.1	22.6	80.8	146.7
St. Mary's	UK	49.92	−6.32	−11.5	18.2	5.4	13.6	−108.4	33.6
Ilfracombe	UK	51.21	−4.11	−23.2	9.7	−12.6	5.0	112.7	38.9
Hinkley Point	UK	51.22	−3.13	−5.6	91.1	11.0	22.8	−12.8	105.3
Avonmouth	UK	51.51	−2.71	92.7	22.6	−26.1	11.5	255.5	88.9
Newport	UK	51.55	−2.99	187.6	93.8	−3.6	11.5	48.4	175.9
Mumbles	UK	51.57	−3.98	−76.1	42.3	−12.2	14.7	−434.1	98.7
Milford Haven	UK	51.70	−5.01	−41.0	17.3	−3.7	8.5	−142.2	99.8
Fishguard	UK	52.01	−4.98	−77.2	10.6	14.0	4.5	81.6	31.6
Barmouth	UK	52.72	−4.05	−7.3	29.4	3.3	10.9	−22.3	69.6
Holyhead	UK	53.31	−4.63	−27.9	10.4	−11.6	8.8	−120.3	40.9
Llandudno	UK	53.33	−3.83	−17.2	56.8	−12.1	24.1	−427.7	235.4
Liverpool	UK	53.45	−3.02	59.5	16.9	−23.6	4.2	−94.3	22.2
Heysham	UK	54.03	−2.92	56.4	15.8	17.2	8.1	385.1	56.7
Port Erin	UK	54.09	−4.77	−5.0	15.0	−38.6	12.1	−229.8	42.8
Workington	UK	54.65	−3.57	−69.8	35.1	−29.5	7.8	−435.4	239.3
Portpatrick	UK	54.84	−5.12	−34.1	34.9	3.9	19.3	−24.6	135.3

Station	Country	Lat (N)	Long(E)	M ₂ TAC	IQR	K ₁ TAC	IQR	δ-HAT	IQR
Millport	UK	55.75	−4.91	21.9	23.9	19.1	25.4	341.7	108.3
Port Ellen (Islay)	UK	55.63	−6.19	−9.5	14.3	−14.8	7.7	−100.4	13.2
Portrush	Ireland	55.21	−6.66	2.4	18.5	47.7	19.2	−37.3	196.2
Malin Head	Ireland	55.37	−7.33	−38.7	24.8	8.4	4.1	−44.0	40.7
Tregde	Norway	58.00	7.57	−17.3	4.9	*	*	−14.1	23.2
Oslo	Norway	59.91	10.73	−41.6	11.2	*	*	−107.2	36.6
Kungsvik	Sweden	59.00	11.13	−30.1	11.5	*	*	−44.7	25.9
Smogen	Sweden	58.35	11.22	−34.6	18.6	*	*	−47.6	65.2
Stenungsund	Sweden	58.09	11.83	−3.5	16.0	*	*	−10.8	22.3
Goteburg-Torshamnen	Sweden	57.68	11.79	−20.6	6.0	*	*	−3.3	35.3
Ringhals	Sweden	57.25	12.11	−17.6	18.4	*	*	−13.1	46.6
Viken	Sweden	56.14	12.58	−18.2	6.7	*	*	−17.5	62.2
Hornbaek	Denmark	56.10	12.47	−16.9	7.4	*	*	20.7	23.6
Esbjerg	Denmark	55.47	8.43	12.1	16.8	−9.9	16.3	56.0	60.6
Cuxhaven	Germany	53.87	8.72	134.9	25.8	−1.3	10.0	218.1	36.6
Delfzijl	Netherlands	53.33	6.93	11.7	35.9	27.6	23.2	140.9	51.7
Den Helder	Netherlands	52.97	4.75	63.3	27.9	−49.0	26.7	139.3	38.6
Hoek van Holland	Netherlands	51.98	4.12	27.3	22.7	−62.1	21.1	−4.7	51.5
Dunkurque	France	51.05	2.37	−142.9	39.5	−28.9	14.7	−340.1	87.5
Le Havre	France	49.48	0.11	−39.6	22.7	0.3	6.2	29.2	45.6
Cherbourg	France	49.65	1.64	−10.2	9.6	−4.8	6.0	40.7	14.5
St. Helier (Jersey)	UK	49.18	−2.12	−145.7	70.8	8.6	18.9	−475.2	163.6
Saint Malo	France	48.64	−2.03	−141.9	20.8	−2.3	12.4	−408.3	49.1
Roscoff	France	48.72	−3.97	−56.6	21.3	−0.1	8.1	39.0	46.0
Le Conquet	France	48.36	−4.78	−2.3	41.8	10.9	11.6	138.6	62.7
Brest	France	48.38	−4.50	−74.0	17.1	3.7	12.1	−166.8	42.6
Port Tudy	France	47.64	−3.45	−24.1	13.5	−15.8	4.9	−19.1	24.2
Donges	France	47.31	−2.09	−26.2	8.4	−7.1	6.7	−4.3	31.1
Cordemais	France	47.28	−1.89	−409.2	113.3	−19.6	4.6	−589.5	146.3
Le Pellerin	France	47.21	−1.77	−625.0	27.6	−12.8	3.1	−983.0	55.6
Nantes-Usine-Brulee	France	47.19	−1.63	−663.0	9.4	−11.8	2.2	−1009.9	32.8
Saint-Gildas	France	47.14	−2.25	57.6	33.5	2.1	18.9	40.2	89.2
Les Sables d’Olonne	France	46.50	−1.79	−17.2	9.7	−0.5	7.3	−44.1	66.3
Bayonne Boucau	France	43.53	−1.51	−21.6	11.8	3.4	3.8	−13.9	15.3
Saint Jean de Luz	France	43.40	−1.68	−9.5	17.3	−1.2	8.0	−52.1	25.0
Bilbao	Spain	43.36	−3.05	−3.3	18.8	11.5	10.9	120.6	37.0
Gijon	Spain	43.56	−5.70	2.3	10.0	10.4	5.4	82.1	29.5
La Coruna	Spain	43.37	−8.40	28.2	17.3	2.9	7.5	200.6	62.5
Vigo	Spain	42.24	−8.73	−6.4	9.2	2.5	9.6	44.2	16.2
Huelva	Spain	37.13	−6.83	10.7	14.4	−33.5	21.9	−14.3	113.0

Station	Country	Lat (N)	Long(E)	M ₂ TAC	IQR	K ₁ TAC	IQR	δ-HAT	IQR
Bonanza	Spain	36.80	−6.34	−7.9	14.1	−11.4	14.1	−43.6	27.8
Cadiz	Spain	36.53	−6.28	75.8	12.8	4.6	2.6	247.3	84.1
Tarifa	Spain	36.00	−5.60	8.4	13.6	14.2	3.7	−3.6	9.0
Funchai	Portugal	32.64	−16.91	124.1	9.5	6.4	2.8	166.0	18.1
Gran Canary	Spain	28.14	−15.41	26.3	12.0	7.4	13.2	106.3	21.2
Tenerife	Spain	28.48	−16.24	−11.4	15.4	5.3	24.5	−73.9	28.1
Barseback	Sweden	55.76	12.90	−22.9	29.7	*	*	−80.6	48.0
Klagshamn	Sweden	55.52	12.89	−25.0	12.4	4.3	17.6	−2.1	26.1
Skanor	Sweden	55.42	12.83	−14.4	5.9	6.1	10.2	21.1	56.7
Gedser	Denmark	54.57	11.93	−0.6	8.5	16.8	16.6	41.3	29.5
Simrishamn	Sweden	55.56	14.36	−1.1	7.8	−0.8	7.0	30.6	28.5
Stockholm	Sweden	59.33	18.08	0.3	3.9	−4.6	5.8	0.2	21.0
Hanko	Finland	59.82	22.98	−1.8	8.0	3.1	5.7	−8.0	16.5
Helsinki	Finland	60.15	24.96	2.1	3.7	17.3	6.9	30.4	29.2
Hamina	Finland	60.56	27.18	−2.7	7.3	20.1	9.2	30.8	17.1
Ceuta	Spain	35.90	−5.32	7.0	13.1	−5.6	10.8	45.1	42.4
Algeciras	Spain	36.12	−5.43	21.0	12.8	11.4	13.0	93.0	40.8
Gibraltar	UK	36.13	−5.35	3.3	6.3	0.9	2.6	3.1	8.1
Malaga	Spain	36.72	−4.42	9.8	6.1	4.6	3.6	27.3	15.9
Venezia	Italy	45.42	12.43	−39.8	21.4	−28.3	21.3	−108.7	65.2
Trieste	Italy	45.65	13.75	29.0	7.8	−2.8	19.6	82.8	38.4
Bakar	Croatia	45.30	14.53	−11.2	5.7	−32.1	20.2	−64.1	67.9

The TAC magnitude is determined by the ensemble average of 12 monthly determinations, and the confidence interval on the determined trend is given by the interquartile range (IQR) of the ensemble. Significant determinations are given in bold text. Entries marked with an “*” indicate locations where analyses failed due to small tidal amplitudes. Units of the TACs and IQRs are in mm m^{−1}.

Table 2.
TAC results for M₂ and K₁ and δ-HAT results at all Atlantic locations.

unreliable. These were not included in averaging process, though at all locations, a minimum of eight of 12 determinations was required to deem a result significant. For more detailed descriptions of the TAC and δ-HAT determinations, please refer to Devlin et al. [10], and the supplementary material of Devlin et al. [8, 9].

4. Selected results

4.1 Data inventory and sources

We now present some of the best results from past studies. Pacific Ocean locations were analyzed in Devlin et al. [9] for individual TACs, whereas Devlin et al. [8] analyzed the combined tidal variability of the δ-HATs, 152 total locations were analyzed in both Pacific studies. Locations are shown in **Figures 3 and 4** (Eastern Pacific and Western Pacific, respectively) with major water basins labeled. The Atlantic Ocean was analyzed in Devlin et al. [10], which calculated both TACs

and δ -HATs, considering a total of 170 locations. Atlantic locations are displayed in **Figure 5** and major basins are labeled. Most of the hourly tide gauge records in the Pacific and Atlantic are obtained from the University of Hawaii’s Sea Level Center

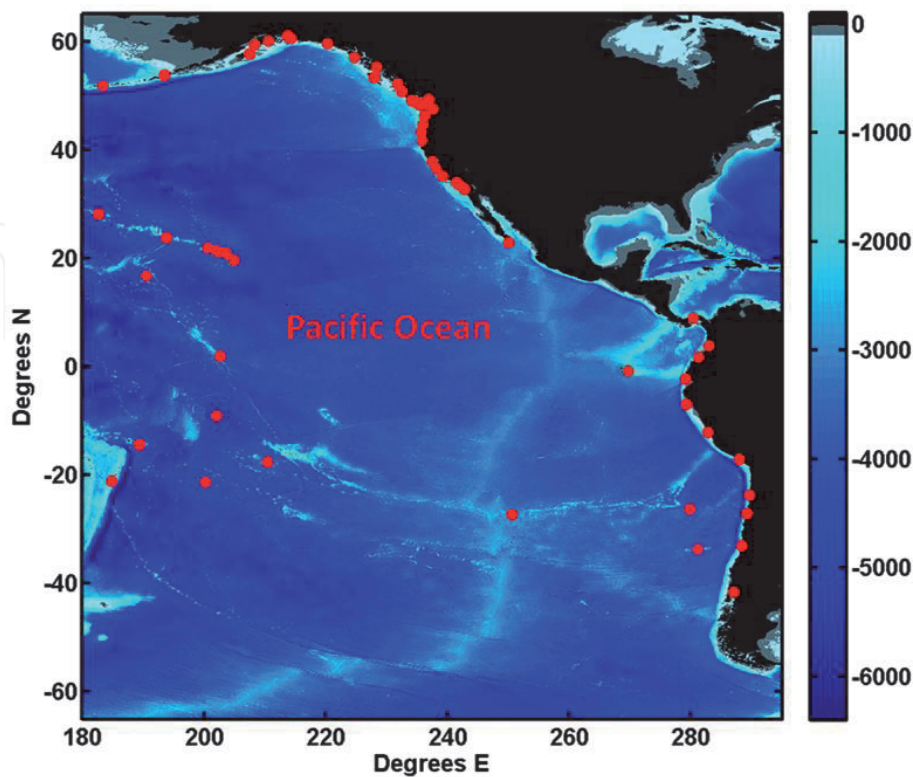


Figure 3.
Red dots indicate gauge locations in the Eastern Pacific [9]. Color bar indicates water depth, in meters. Areas with a depth less than 100 m are shaded gray, and land is black.

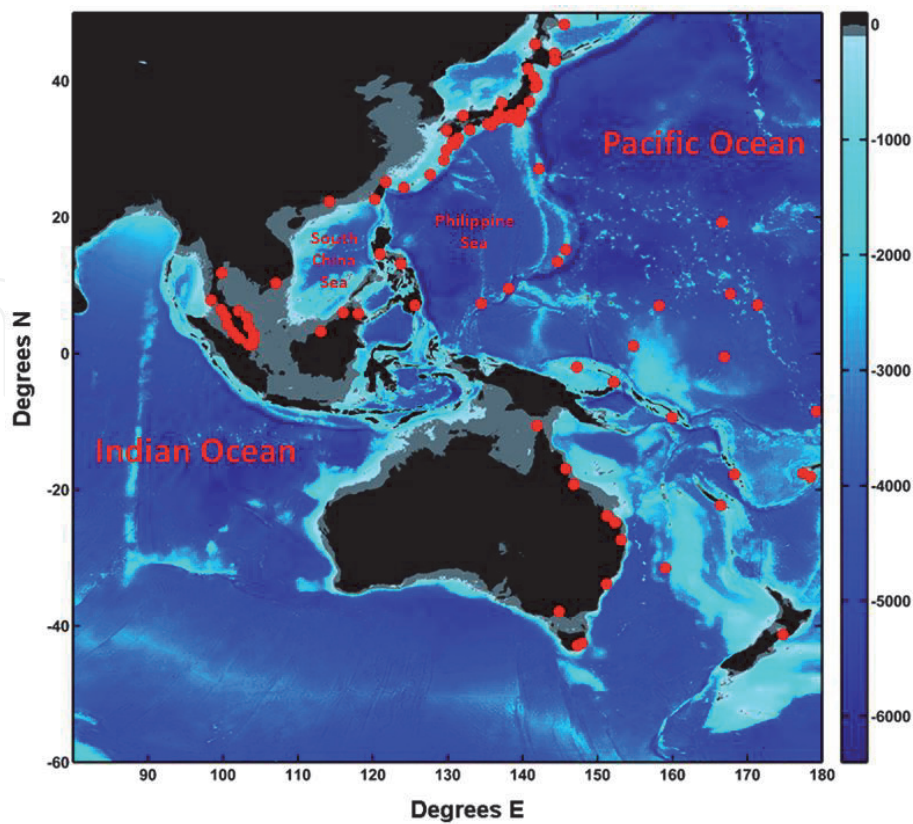


Figure 4.
Red dots indicate gauge locations in the Western Pacific [9]. Color bar indicates water depth, in meters. Areas with a depth less than 100 m are shaded gray, and land is in black.

(UHSLC), with additional data from the following agencies: The Japanese Oceanographic Data Center (JODC); Canada's Fisheries and Ocean office (FOC); Australia's National Tidal Center (AuNTC), and the remainder from the Global Extreme Sea Level Analysis dataset, 2nd edition (GESLA [61]; www.gesla.org), an archiving project that has gathered high-frequency water level data into a single standardized data format from multiple worldwide monitoring agencies. Finally, a close regional study of the tidal variability (individual and combined) of the Hong Kong tide gauge network (12 gauges) was performed in Devlin et al. [11]; this data was obtained from the Hong Kong Observatory (HKO) and the Hong Kong Marine Department (HKMD); locations are shown in **Figure 6**. For the Pacific and Hong Kong studies, the four largest tidal constituents (M_2 , S_2 , K_1 , and O_1) and their combinations (δ -HAT) were considered. The Atlantic study also considered four more tides (N_2 , K_2 , P_1 , and Q_1), and the combined δ -HAT considered here involved all eight components. However, for the sake of brevity in this chapter, only the largest semidiurnal (M_2) and diurnal (K_1) tide results will be discussed, along with δ -HAT determinations.

In all Pacific plots, the magnitude of the TACs or δ -HATs are indicated by the color intensity of the dots according to the scale shown in the legend; positive TACs are in shades of red, negative TACs are in shades of blue. For a gauge with an insignificant TAC (signal-to-noise ratio less than 2.0), the dots are white. In the Atlantic and Hong Kong results, red markers indicate positive TACs and blue markers indicate negative TACs, with magnitudes proportional to marker size, as shown in the legend, and insignificant results are shown as black dots. These values provide a measure of the tidal response, normalized to a 1 m MSL rise. In the TAC plots, the green and yellow background fields show the mean value of tidal

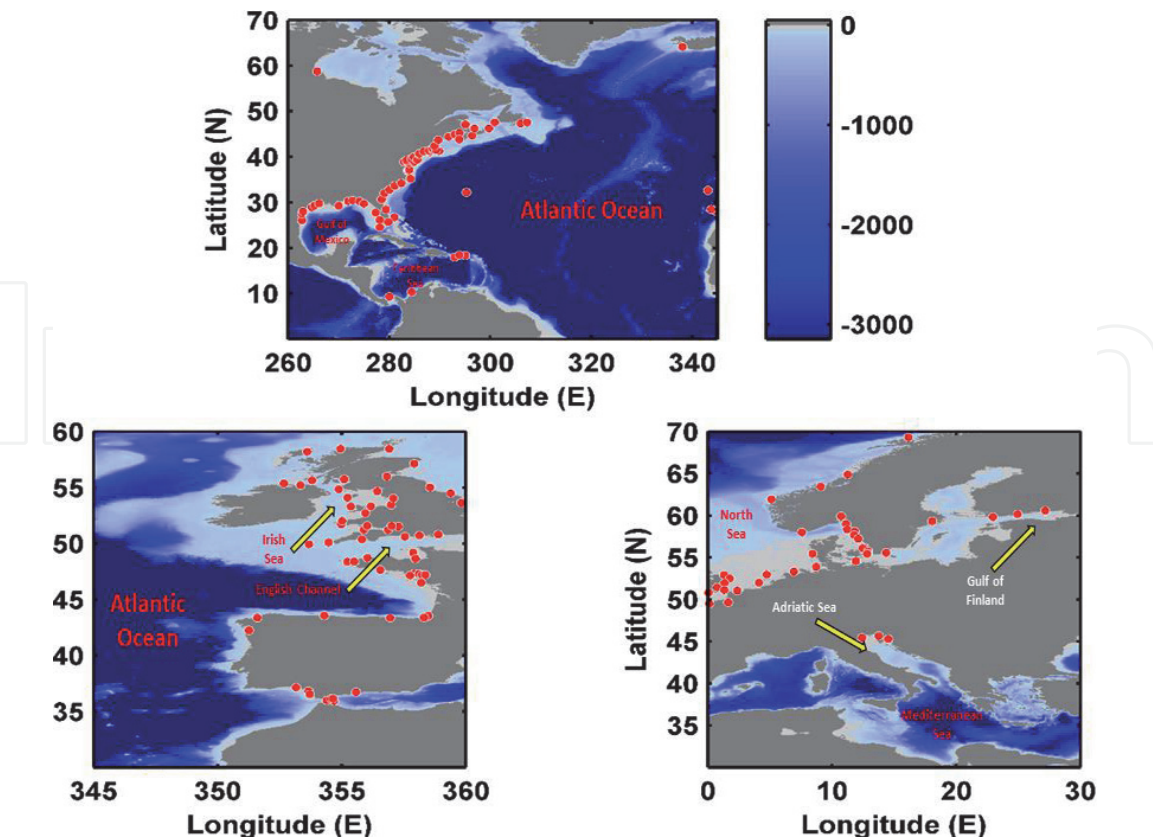


Figure 5. Gauge locations analyzed in the Atlantic Ocean. The colored background shows water depth, in units of meters [10].

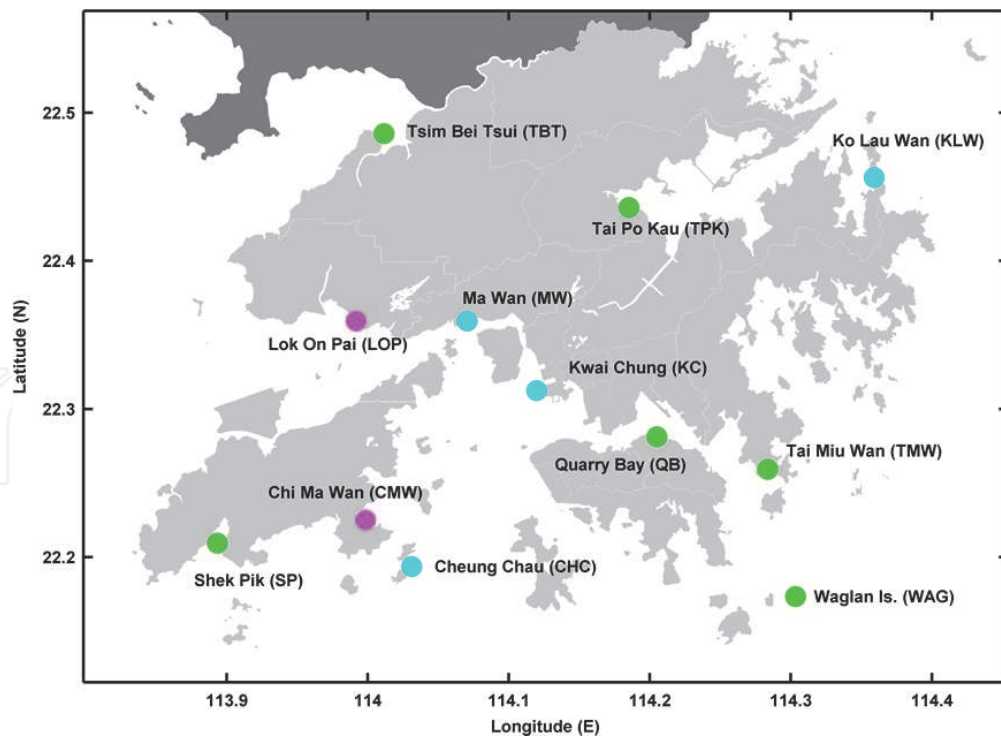


Figure 6.
 Tide gauge locations in Hong Kong used in this study [11]. Green markers indicate active gauges provided by the Hong Kong Observatory (HKO), light blue markers indicate gauges provided by the Hong Kong marine department (HKMD), and red markers indicate historical gauges (once maintained by HKO) that are no longer operational.

amplitudes over the satellite altimetry record (1993–2014), using a tidal solution from the TPXO7.2 tide model [62, 63].

4.2 Pacific results

4.2.1 Pacific M_2 TACs

The M_2 TACs do not reveal any coherent basin-wide patterns of variability, however, there are localized features of interest. In the Eastern Pacific (**Figure 7**), river-influenced gauges, such as San Francisco, California, Astoria, Oregon (labeled as “SF” and “AST” on the map) exhibit strong negative TACs. Strongly positive M_2 TACs are observed at many Hawaiian and Alaskan gauges. Other locations show only weak or isolated correlations. At one gauge of note, Puerto Montt in far southern Chile (labeled as “PM” in **Figure 7**), there is an exceptionally large negative M_2 TAC, greater than -500 mm m^{-1} . There are a higher number M_2 TACs in the Western Pacific than in the Eastern Pacific, but again the relevant variability is local (**Figure 8**). M_2 TACs are negative for the majority of Japan and Taiwan, some exceeding -100 mm m^{-1} . However, some large positive M_2 TACs are at isolated locations, such as at Okada (labeled as “OKA” in **Figure 8**) and in Tokyo harbor (“TOK”). At Hong Kong (“HK”), one of the largest positive M_2 TACs is found (discussed in further detail below). Most significant positive TACs are south of the equator, and most negative TACs are north of the equator. The correlations at nearly all gauges in Malaysia (-40 to -150 mm m^{-1}) and in the Philippines (-80 to -145 mm m^{-1}) are strongly negative. Finally, Honiara (“HON”) in the Solomon Islands and Rabaul, Papua New Guinea (“RAB”) have small mean M_2 amplitudes ($\sim 50 \text{ mm}$) but display large relative correlations.

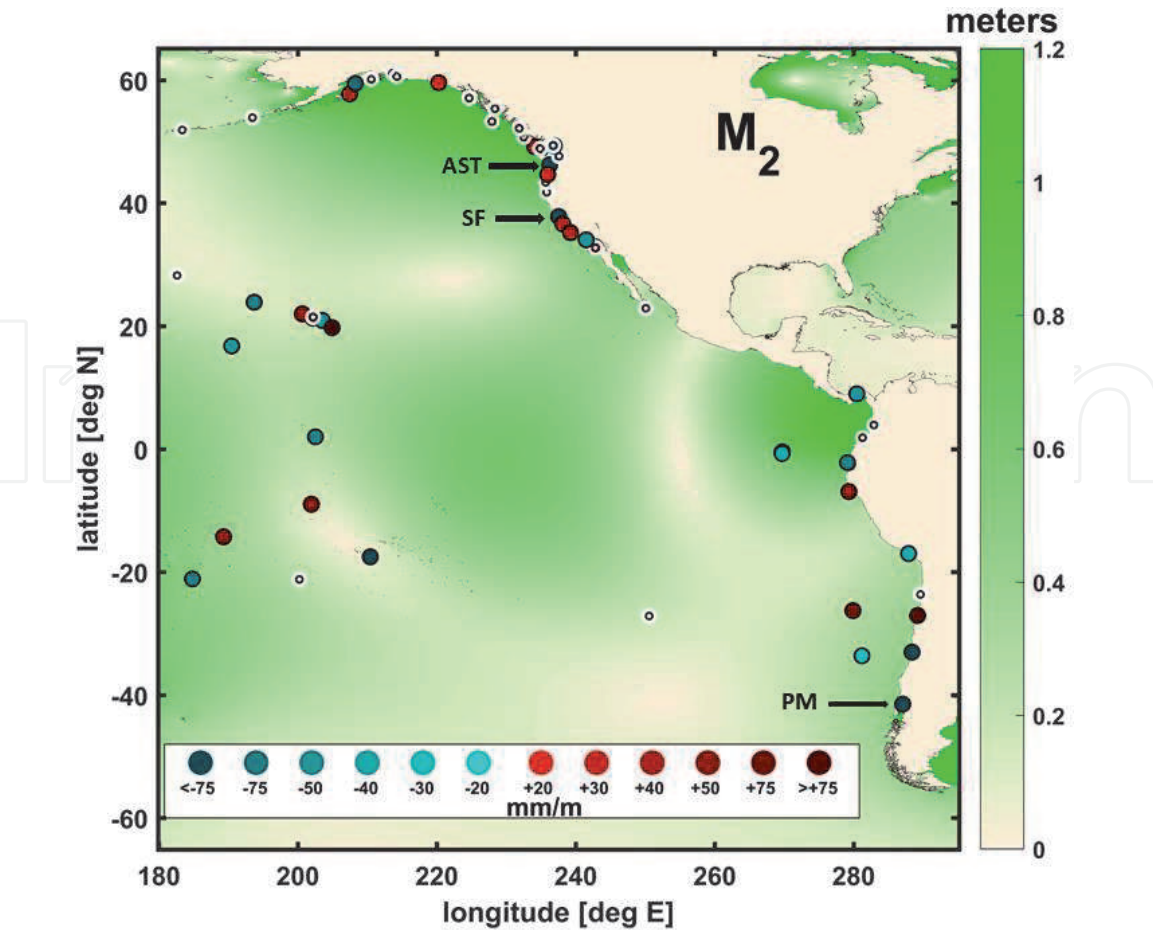


Figure 7. M_2 TAC map in the Eastern Pacific [9], showing changes in amplitude (per m MSL rise). Map background shows mean tidal amplitudes (meters, green color scale) from the ocean tidal model of TPXO7.2 [62, 63]. Red and blue colored markers show positive and negative TACs, respectively. The magnitudes are indicated by color intensity, as shown by legend at the bottom, in units of mm of tidal change per meter of sea level rise (mm m^{-1}). TACs are only plotted if the ratio of the 95% confidence limit of the trends has a signal-to-noise ratio of >2.0 . Statistically insignificant values are indicated by white circles. Maps were generated using MATLAB version R2011a (www.mathworks.com).

4.2.2 Pacific K_1 TACs

K_1 tidal anomaly correlations also reveal some regions of regionally coherent behavior but no basin-scale patterns. In the Eastern Pacific (**Figure 9**), the river-influenced gauges of San Francisco, California (labeled “SF” in **Figure 9**), and Astoria, Oregon (“AST”) show TACs that are strongly negative, as was true for M_2 . However, slightly negative or insignificant K_1 TACs are observed along the rest of the US west coast (**Figure 9**). Fewer significant K_1 TACs are observed in Alaska and Hawaii than was seen for M_2 . In South America, Puerto Montt, Chile (“PM”) shows a very strong negative K_1 TAC, like M_2 . A larger number of significant K_1 TACs are found in the Western Pacific (**Figure 10**). As with M_2 , most coastal Japan gauges exhibit negative TACs, and there is a very large positive TAC in Hong Kong (labeled “HK” in **Figure 10**). In the Southwest Pacific, large positive TACs occur at both island and shelf stations, while significant negative TACs are mainly observed at island gauges, and in Malaysia and Thailand. Almost all significant negative TACs are north of ~ 10 degrees South.

4.2.3 Pacific δ -HATs

In the Eastern Pacific (**Figure 11**), significant δ -HATs are isolated. San Francisco, California (labeled “SF” in **Figure 11**) and Astoria, Oregon (“AST”)

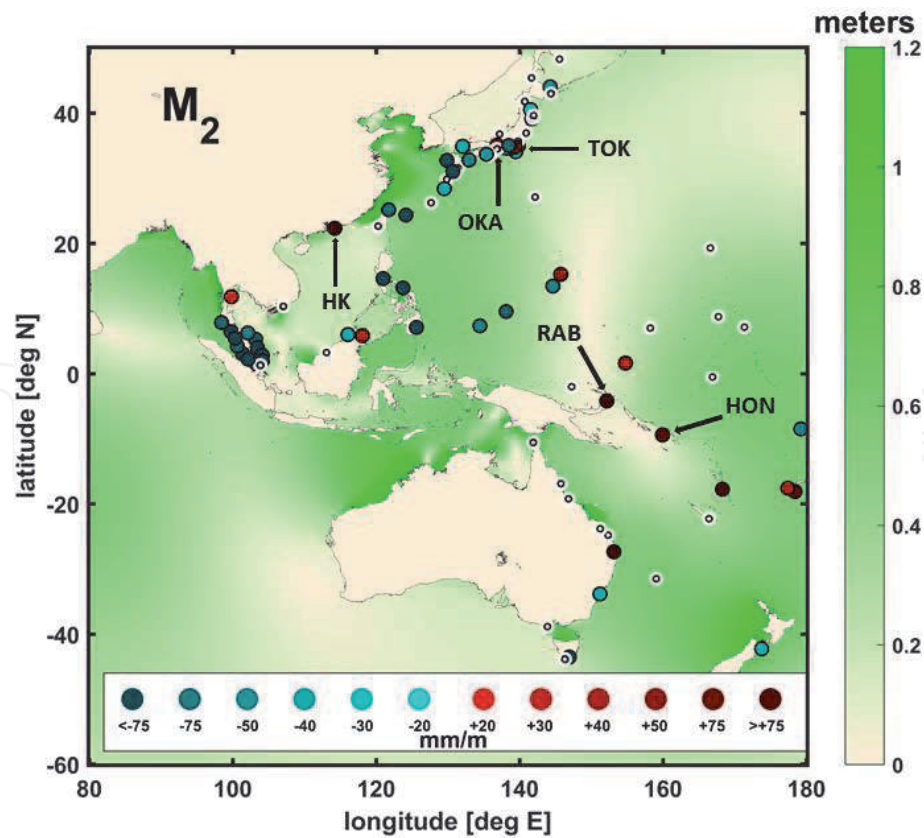


Figure 8.
 M_2 TAC map in Western Pacific [9] showing changes in amplitude anomaly trends (for a 1-meter MSL rise); symbols and backgrounds are as in Figure 7; units of red and blue markers are mmm^{-1} , and units of the backgrounds are meters. Maps were generated using MATLAB version R2011a (www.mathworks.com).

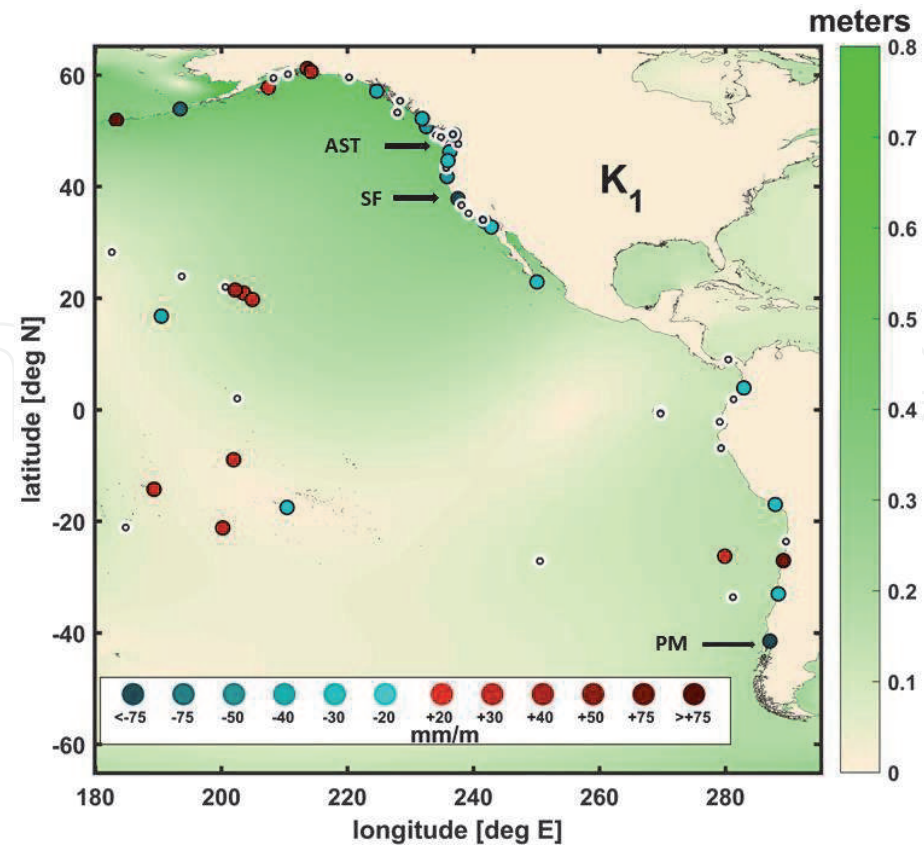


Figure 9.
 K_1 TAC map in Eastern Pacific [9] showing changes in amplitude anomaly trends (for a 1-m MSL rise); symbols and backgrounds are as in Figure 7; units of red and blue markers are mmm^{-1} , and units of the backgrounds are meters. Maps were generated using MATLAB version R2011a (www.mathworks.com).

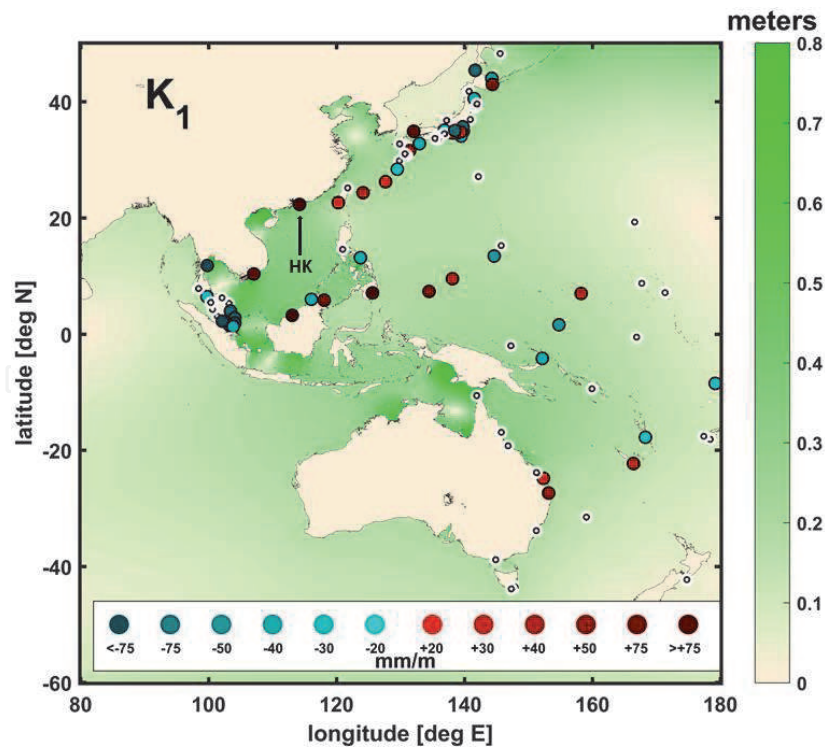


Figure 10. K_1 TAC map in Western Pacific [9] showing changes in amplitude anomaly trends (for a 1-m MSL rise); symbols and backgrounds are as in Figure 7; units of red and blue markers are mm m^{-1} , and units of the backgrounds are meters. Maps were generated using MATLAB version R2011a (www.mathworks.com).

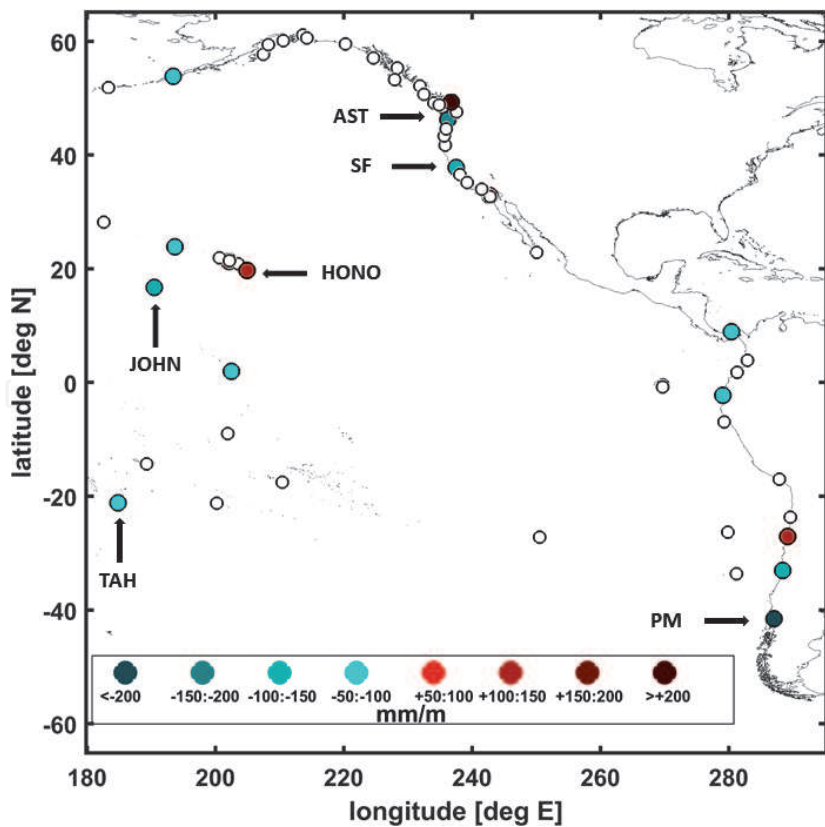


Figure 11. Color scale map of the eastern Pacific δ -HAT determinations (in mm m^{-1}), based on the combined M_2 , S_2 , K_1 , and O_1 detrended tidal variations [8]. Red and blue colored markers show positive and negative δ -HATs, respectively. Un-colored, open circles indicate that the calculated δ -HATs was not significant ($p > .05$). Maps were generated using MATLAB version R2011a (www.mathworks.com).

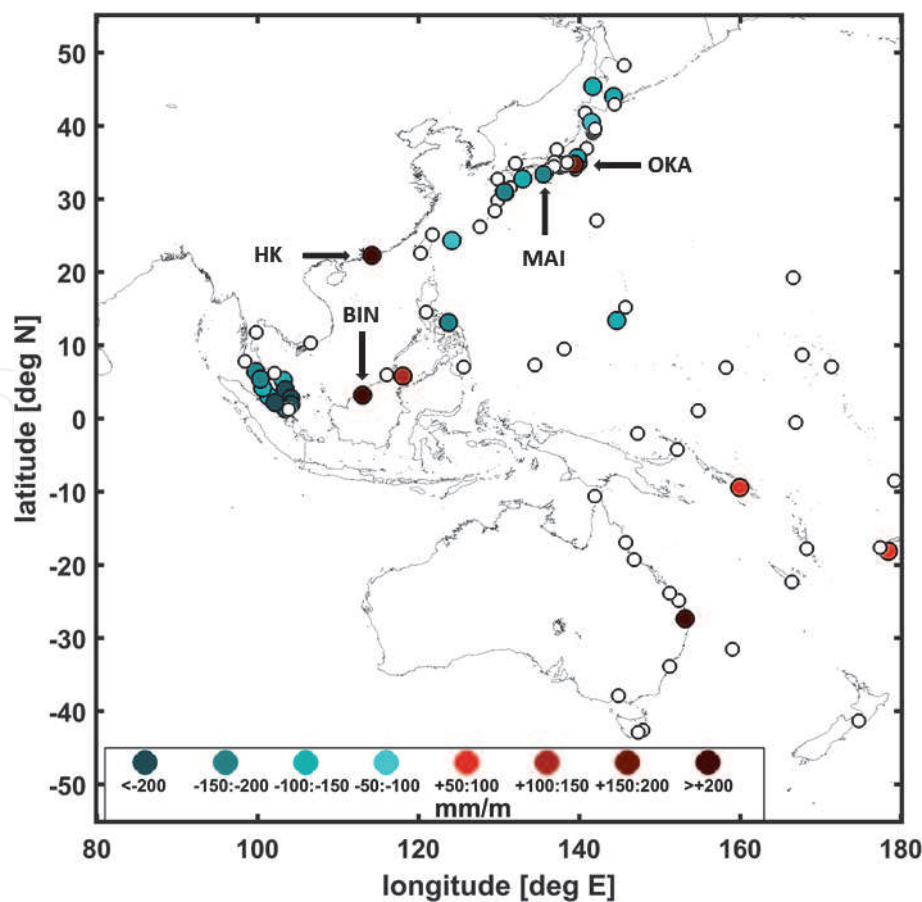


Figure 12.
Color scale map of the Western Pacific δ -HAT determinations (in mm m^{-1}), symbols and colors as in Figure 11 [8]. Maps were generated using MATLAB version R2011a (www.mathworks.com).

exhibit δ -HAT values of -146 - and -257-mm m^{-1} , respectively. Honolulu (“HONO”) and Hilo, Hawaii have positive values of $+139$ - and $+147\text{-mm m}^{-1}$, respectively. Along the coast of South America, there is an anomalously large negative anomaly correlation at far-southern Puerto Montt, Chile (“PM”), with a δ -HAT value of -963 mm m^{-1} . Elsewhere in the Eastern Pacific of note, Johnston Island (“JOHN”) and Papeete on the island of Tahiti (“TAH”), exhibit large negative δ -HATs of -117 mm m^{-1} and -95 mm m^{-1} , respectively.

The δ -HAT correlations are more significant in the Western Pacific (Figure 12). Eleven gauges in Japan show negative δ -HATs, seven of which are greater than -100 mm m^{-1} , with a maximum negative value of -351 mm m^{-1} occurring at Maisaka (labeled “MAI” in Figure 12). Only two significant positive δ -HATs are observed in Japan, at Okada (“OKA”) with a value of $+159$. At Western Pacific islands, results are mixed, with moderate positive δ -HATs and moderate negative δ -HATs both observed. Within the South China Sea, the distribution of δ -HATs is complex. An anomalously large positive δ -HATs is observed at Hong Kong (“HK”; $+665\text{ mm m}^{-1}$) and at Bintulu, Malaysia (“BIN”; $+615\text{ mm m}^{-1}$). Both sides of the Malay peninsula exhibit strongly negative δ -HATs. The Malacca Strait on the west side of the peninsula has δ -HATs of approx. -70 to -220 mm m^{-1} , and the Gulf of Thailand on the eastern side shows δ -HATs of approx. -130 to -290 mm m^{-1} ; a common feature is that both sides show gradual increases in magnitude from the northern reaches to the southern tip of the Malay Peninsula.

4.3 Atlantic results

4.3.1 Atlantic M_2 TACs

Figure 13a–c show the M_2 results. In North America (**Figure 13a**), the M_2 TACs show a dipole-like pattern. Both sides of the Florida Peninsula show TACs that are consistently positive. However, they are moderately negative in the Western Gulf of Mexico. Farther north along the US Atlantic coast, a strong concentration of negative TACs are seen from the Florida panhandle to Virginia in the Sargasso Sea, with the strongest correlation in Wilmington, North Carolina (-211 mm m^{-1} ; labeled “WIL” in **Figure 13**). Positive TACs are seen in the Chesapeake and Delaware Bays, New York City, New York (“NYC”), and Bar Harbor, Maine (“BH”). Finally, TACs in the Gulf of Maine and into the Bay of Fundy are strongly negative, reaching a magnitude of -259 mm m^{-1} at St. John, Canada (“STJ”). In Europe, the TAC patterns are somewhat more consistent (**Figure 13b, c**). Negative TACs are seen in most of the English Channel and the Irish Sea, and in the eastern parts of the North Sea. Conversely, positive TACs are found at inland semi-enclosed locations in England such as the Severn estuary; being largest at Avonmouth (“AVON”), farther north at Liverpool (“LIV”), and along the southern coast of the North Sea.

4.3.2 Atlantic K_1 TACs

Diurnal components are generally smaller than semidiurnal constituents in the Atlantic, and TACs are also generally lower magnitude (usually $< \pm 100 \text{ mm m}^{-1}$)

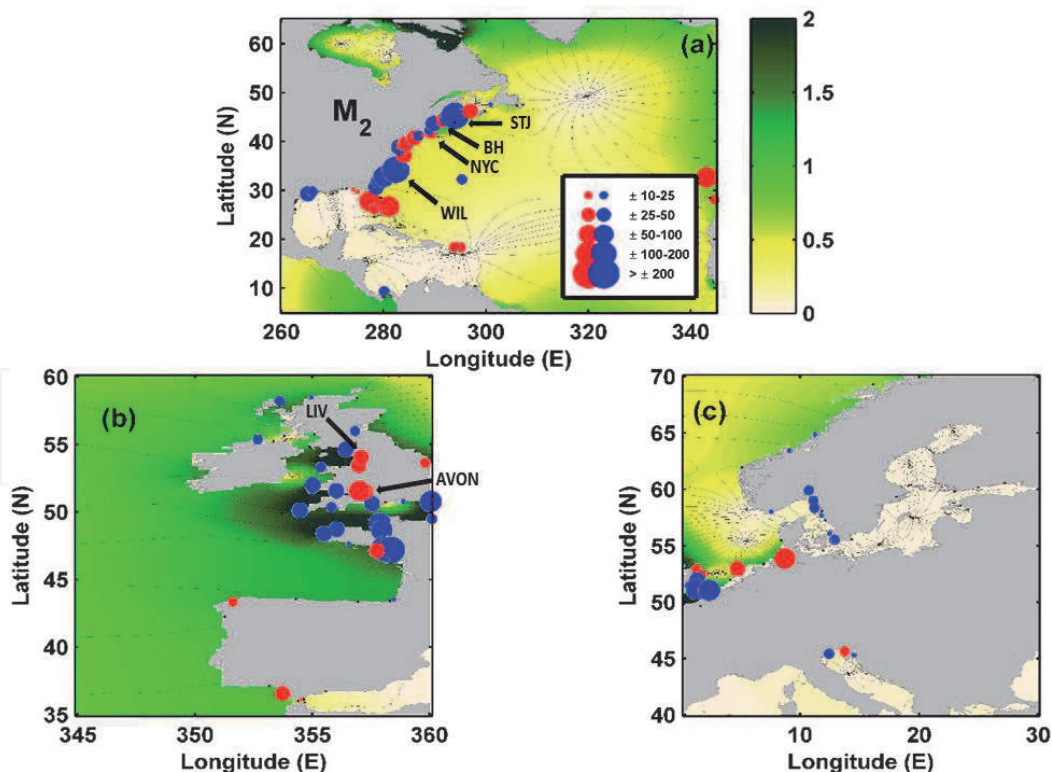


Figure 13.

M_2 TAC Atlantic Ocean maps [10]. North American locations are shown in (a), Western Europe and United Kingdom locations are shown in (b), and Eastern Europe locations are shown in (c). Red markers indicate positive TACs and blue markers indicate negative TACs, with magnitudes proportional to marker size, as shown in the legend in (a). Black markers indicate insignificant results. Green-and-yellow background maps show the global tidal solutions over the satellite era, taken from the TPXO7.2 solution [62, 63], with green and yellow colors giving the tidal amplitudes, and black lines showing tidal phases. Maps were generated using MATLAB version R2011a (www.mathworks.com).

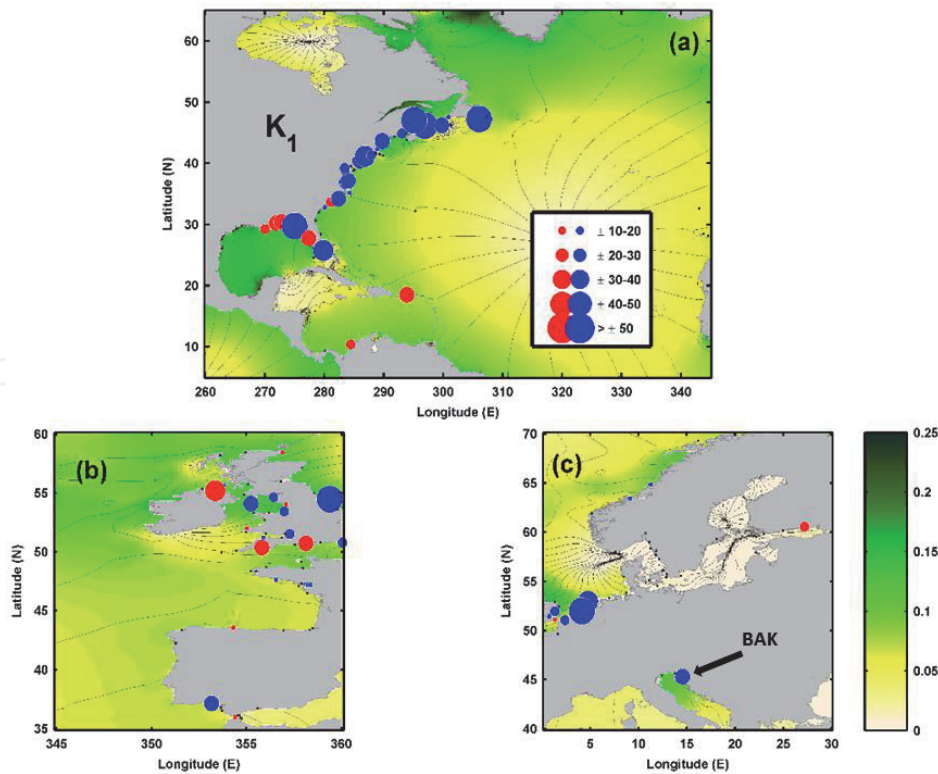


Figure 14.
K₁ TAC Atlantic Ocean maps [10]. North America locations are shown in (a), Western Europe and United Kingdom locations are shown in (b), and Eastern Europe locations are shown in (c). Markers and background maps are as described in Figure 13. Maps were generated using MATLAB version R2011a (www.mathworks.com).

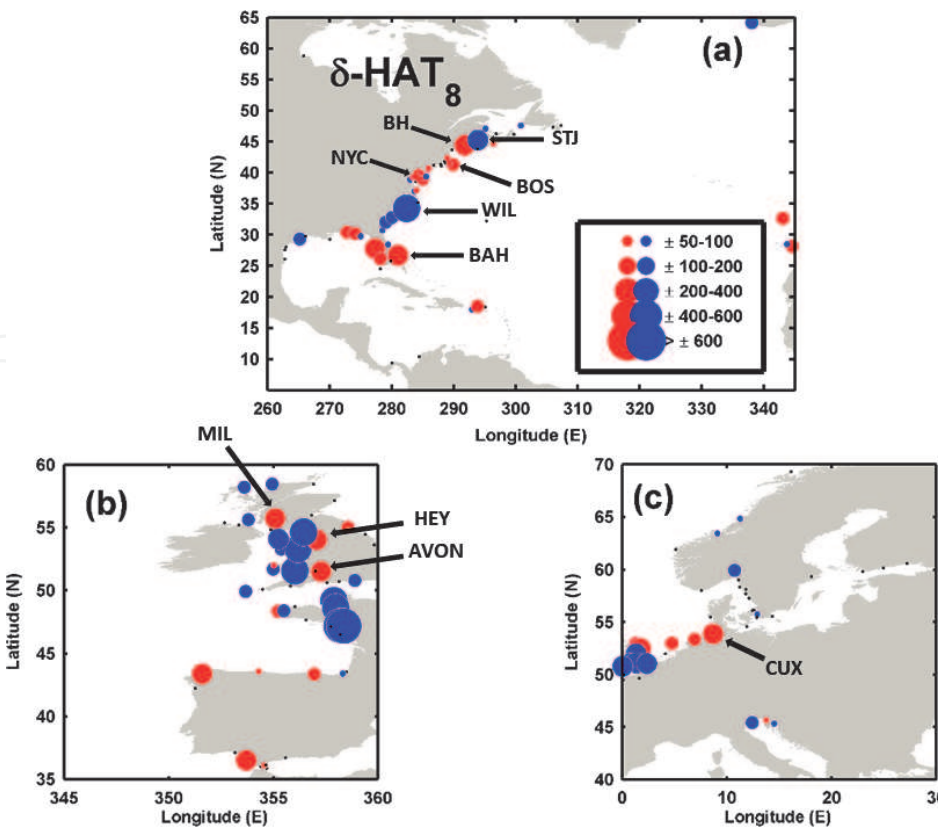


Figure 15.
δ-HAT8 Atlantic Ocean maps [10], showing combined variability of eight largest gravitational tides ($M_2 + S_2 N_2 + K_2 + K_1 + O_1 + P_1 + Q_1$). North American locations are shown in (a), Western Europe and United Kingdom locations are shown in (b), and Eastern Europe locations are shown in (c). Markers are as described in Figure 13. Maps were generated using MATLAB version R2011a (www.mathworks.com).

and less often significant. However, there are still some regions of interest. The K_1 tide (**Figure 14a**) has TACs that are consistently negative along the North American coast from Florida through maritime Canada. However, the TACs in the Gulf of Mexico are mainly positive, as well as in the Caribbean. K_1 has some isolated positive TACs in Europe in the western English Channel, while the eastern Channel has a concentration of negative TACs (**Figure 14b**). There is a negative TAC at Bakar, Croatia (labeled “BAK” in **Figure 14**) at the end of the Adriatic Sea, where a large diurnal amplification occurs, and a small positive TAC at the end of the Gulf of Finland, where a diurnal amplification of the otherwise small Baltic tides also occurs (**Figure 14c**).

4.3.3 Atlantic δ -HATs

The calculation of the δ -HATs in the Atlantic use an eight-tide combination instead of the four-tide combination used in the Pacific, as detailed in Devlin et al. [10]. Results in North America (**Figure 15a**) are generally positive in the eastern Gulf of Mexico, Puerto Rico, and a large magnitude δ -HAT is seen in the Bahamas (+323 mm m⁻¹; labeled “BAH” in **Figure 15**). New York City, New York (“NYC”), Boston, Massachusetts (“BOS”), Bar Harbor, Maine (“BH”), and parts of the Delaware Bay also are strongly positive. Strong negative δ -HATs are found from Florida to Wilmington, North Carolina (−413 mm m⁻¹; “WIL”), and at St. John at the head of the Bay of Fundy (−378 mm m⁻¹; “STJ”). In Europe (**Figure 15b, c**), strong positive δ -HATs are found in the southern North Sea at Cuxhaven, Germany (+219 mm m⁻¹; “CUX”) and in the Netherlands. Three locations within semi-enclosed regions of the Irish Sea show the strongest positive δ -HATs; at Avonmouth located at the head of the Severn Estuary (+256 mm m⁻¹; “AVON”), and at Heysham (“HEY”) and Millport (“MIL”; +385 and +341 mm m⁻¹, respectively). However, there are mainly negative δ -HATs seen in the rest of the UK, including most of the English Channel.

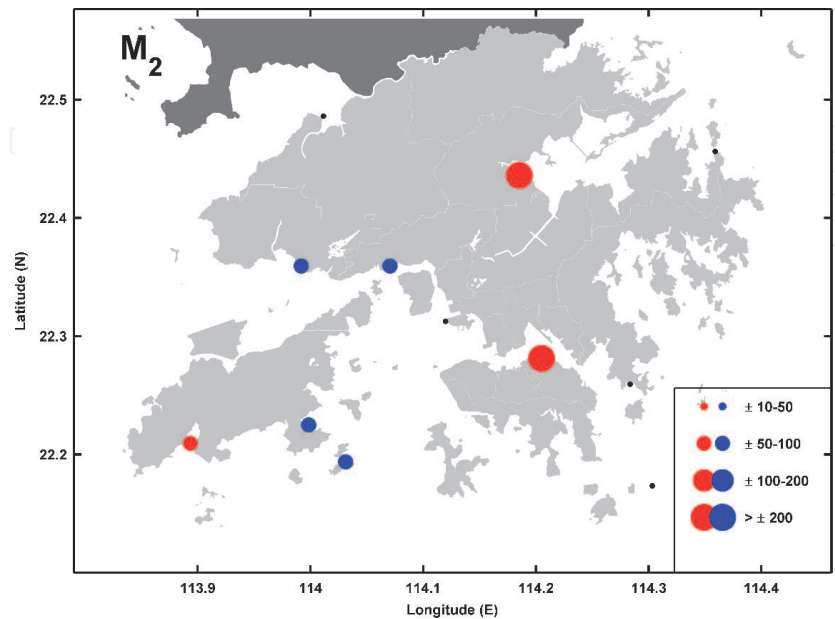


Figure 16. Tidal anomaly correlations (TACs) of detrended M_2 amplitude to detrended MSL in Hong Kong [11], with the marker size showing the relative magnitude according to the legend, in units of mm m⁻¹. Red/blue markers indicate positive/negative TACs, and black markers indicate TACs which are not significantly different from zero. Maps were generated using MATLAB version R2011a (www.mathworks.com).

4.4 Hong Kong results

4.4.1 TAC and δ -HAT results

We now move from basin-wide surveys to a more tightly focused regional analysis of the Hong Kong waters, where 12 closely spaced tide gauges are available. For gauge names and locations, the reader is directed to refer to **Figure 6**.

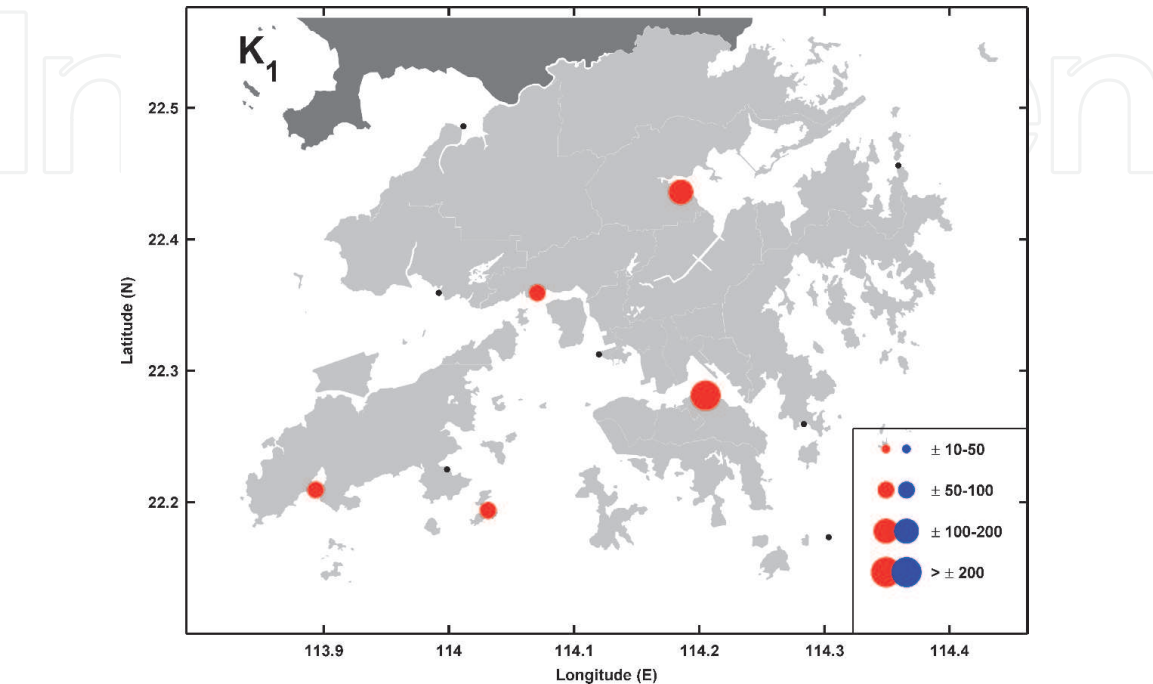


Figure 17.
*Tidal anomaly correlations (TACs) of detrended K_1 amplitude to detrended MSL in Hong Kong [11], with the marker size showing the relative magnitude according to the legend, in units of mm m^{-1} . Markers are as in **Figure 16**. Maps were generated using MATLAB version R2011a (www.mathworks.com).*

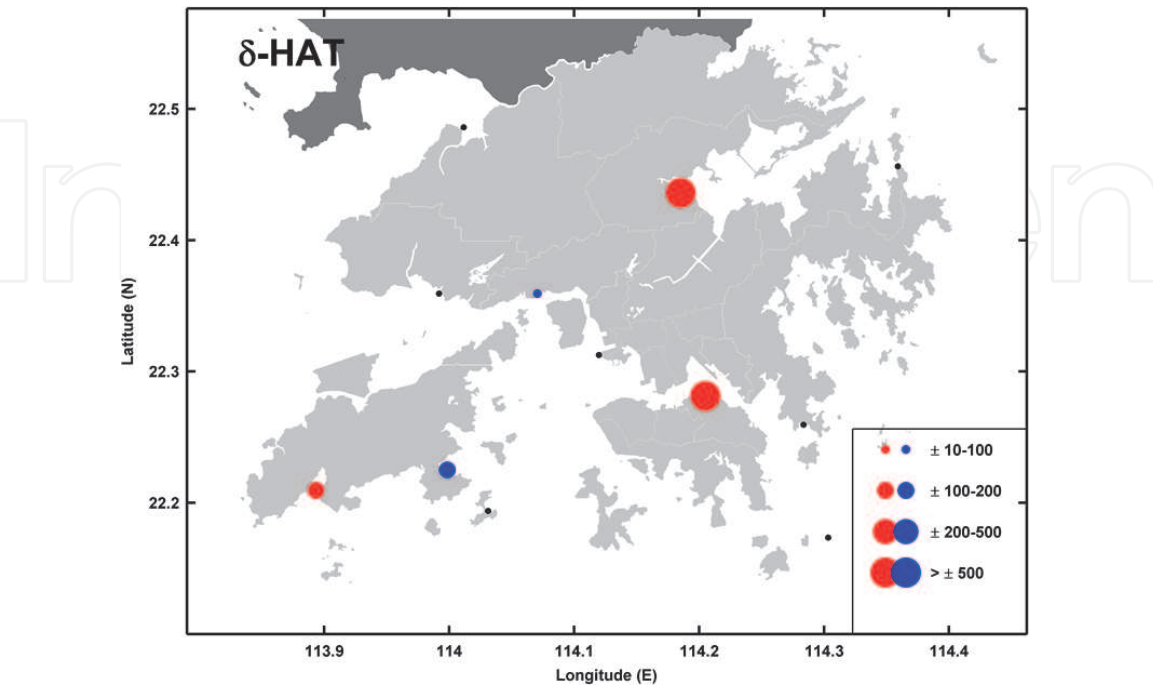


Figure 18.
 *δ -HAT map in Hong Kong [11], with the marker size showing the relative magnitude according to the legend, in units of mm m^{-1} . Markers are as in **Figure 16**. Maps were generated using MATLAB version R2011a (www.mathworks.com).*

The strongest positive M_2 TACs are seen at Quarry Bay ($+218 \text{ mm m}^{-1}$), and at Tai Po Kau ($+267 \text{ mm m}^{-1}$), with a smaller positive TAC seen at Shek Pik (**Figure 16**). In the waters west of Victoria Harbor, all gauges except Kwai Chung exhibit moderate negative TACs. The diurnal TACs in Hong Kong generally exhibit a larger-magnitude and more spatially coherent response than semidiurnal TACs. Like M_2 , the strongest K_1 values in Hong Kong (**Figure 17**) are seen at Quarry Bay ($+220 \text{ mm m}^{-1}$) and Tai Po Kau ($+190 \text{ mm m}^{-1}$).

The TACs are widely observed in Hong Kong, but the δ -HATs are only of significance at a few locations (**Figure 18**). Five stations exhibit significant δ -HAT values, with Quarry Bay and Tai Po Kau having very large positive magnitudes ($+665 \text{ mm m}^{-1}$ and $+612 \text{ mm m}^{-1}$, respectively), and Shek Pik having a lesser magnitude of $+138 \text{ mm m}^{-1}$. Conversely, Ma Wan and Chi Ma Wan exhibit moderate negative δ -HAT values (approx. -100 mm m^{-1}). The remainder of gauges (which are mainly open-water locations) have statistically insignificant results for the combined tidal amplitudes, even where some large individual TACs were observed. This shows that the combined tidal amplitude effect as expressed by the δ -HATs is most important in semi-enclosed harbors.

5. Summary and discussions

5.1 Summary of results

We have presented the salient features of several past studies, covering nearly all the global ocean, in efforts to understand the nature of tidal variability associated with mean sea level variability. Here, we will present a quick summary of the results, and then discuss some similarities of all results.

In the Pacific Ocean, out of 152 tide gauges considered, M_2 TACs are significant at 89 gauge, and K_1 TACs are significant at 76 gauges. For the combined tidal variability of these four tides, 54 stations ($\sim 35\%$) are significantly correlated to variations in sea-level, with δ -HATs $> \pm 50 \text{ mm m}^{-1}$ (i.e., $> \pm 5\%$ of the sea level perturbation). In the Atlantic Ocean, 104 gauges have significant TACs, and for K_1 , 62 locations exhibit TACs that are significant. For the combination of the eight largest tides, there is a near even mix in the Atlantic of positive (40) and negative (47) δ -HATs. Finally, in Hong Kong, mixed results were seen for individual TACs, but δ -HATs were only important at a few semi-enclosed harbor locations, namely Quarry Bay (Victoria Harbor), and Tai Po Kau, where the largest positive feedbacks worldwide were seen.

5.2 TAC and δ -HAT distributions and patterns

There are a few commonalities seen in both the Pacific and Atlantic basins. First, the yearly averaged response of the tides due to correlated MSL changes (TACs) show an overall mixed pattern of positive and negative responses. There is no apparent ocean-wide pattern that might suggest a single cause to the variability, but some regionally coherent patterns of variability are apparent. While many gauges show an increase in tidal amplitudes with increasing MSL (positive TAC), many exhibit a decrease (negative TAC), which suggests a variety of mechanisms may be at play. Second, individual TACs are more widespread, being significant at a larger number of tide gauges, but δ -HATs are only significant at a smaller number of locations. This is because some individual TACs can be partially canceled out by other individual TACs, yielding an overall tidal variability that is less intense. However, some locations do see a reinforced trend when considering all major tidal

constituents, yielding strong δ -HATs, and both positive and negative combinations are observed. Third, the largest δ -HATs tend to be located in coastal locations and not at open-ocean island locations. Many estuarine regions see the largest δ -HATs and most of the strongest individual TACs, as can be seen from the results in Hong Kong, which is located in the Pearl River Delta, and had the largest magnitude results. Other locations of note that are in estuarine environments include gauges in or near the Severn estuary in England, the Loire estuary in France, Astoria, Oregon, in the Columbia River Delta, and San Francisco Bay, California, which is fed by the Sacramento River.

There are some isolated locations do not fit this generalization, such as Hawaii, where the large significant positive values of δ -HATs at Honolulu and Hilo are mainly due to the M_2 TAC, but this is likely related to the changing phase of the internal tide [37]. On the western side of the South China Sea, gauges in Malaysia exhibit large negative δ -HATs related to the seasonal variability in tides due to stratification, seasonal monsoon winds and water depth [64]. In other shallow, semi-enclosed regions, such as the North Sea, increasing sea-level has amplified tides on the German/Dutch coast over the past 50 years due to reduced frictional effects [65].

The regional case of Hong Kong is particularly interesting. Only a few locations showed strong δ -HATs, and these are in sensitive harbor locations. Hong Kong has had a long history of land reclamation to accommodate an ever-growing infrastructure and population, including the building of a new airport island (Chep Lap Kok), new land connections, channel deepening to accommodate container terminals, and many bridges, tunnels, and “new cities”, built on reclaimed land. All of these may have changed the resonance and/or frictional properties of the region. Tai Po Kau has also had some land reclamation projects that have changed the coastal morphology and may have modulated the tidal response. Other locations in Hong Kong did not show such extreme variations, so these variations appear to only be amplified in harbor areas.

5.3 Importance of combined tidal variability and nuisance flooding

The individual TACs reveal valuable information about the complex frequency-dependent response of the ocean. However, the metric that is most important for coastal planning is how all tidal components can combine and interact under changing MSL to increase local flood frequency and intensity. The δ -HATs provide an effective parameter to measure the full effect of changing tides, as they incorporate multiple tidal variabilities simultaneously. It is therefore of the greatest interest for the future of coastal flooding to find where all tides can change in the same direction, and the occurrence of the largest δ -HATs are likely dominated by local effects, such as a combination of natural and human-induced water level changes in sensitive harbor areas. If regional or amphidromic scales were dominant, then more coherent regional changes would be observed in the δ -HATs. If the changes in a local environment are favorable, all major tides can be enhanced and reinforced, and this may be via changes in tidal velocity and phase that better “tune” the response to yield higher water levels.

The impact of large δ -HATs on coastal and estuarine locations as sea level rises may be best demonstrated via the concept of nuisance flooding. Nuisance flooding refers to minor flooding events that happen at high tide without a strong storm surge, also called “sunny day flooding” [66]. Such events may also be induced by minor storm tides, Rossby waves [67] or pluvial flooding [68]. Nuisance floods are usually non-destructive individually, yet frequent occurrences can cause cumulative financial and societal impacts to coastal regions. Roads may flood more,

disrupting logistics and supply chains [69]. Sewers and drainage systems may overflow [70], increasing public health risks [71]. Flood probabilities and cumulative hazards are likely to further increase under future sea level rise scenarios, with an increased effect seen during El Nino events [5, 6, 72]. Most previous examinations of nuisance flooding only consider a changing MSL and a static tidal range, but some studies have demonstrated the importance of tidal changes leading to increased inundation, such as at Boston [73]. In some locations, secular changes to tidal range far outpace sea-level rise (e.g., Wilmington, North Carolina; [35]), and help drive flood risk. Moreover, since storm surge is a long wave, factors affecting tides can also alter storm surge [34, 74].

Figure 19 shows a simple representation of nuisance flooding with four cases presented. In the past when MSL was stable, it would take a storm surge (dark blue) to surpass local flooding levels (situation [a]), but under higher MSL conditions of the present day with unchanged tides, inundation can occur at high tide, especially on higher spring tides (situation [b]). If tides are not stationary with MSL rise, two additional situations are possible. If MSL increase leads to a slightly dampened high tide, then nuisance flooding will still happen, but will not be as extreme (situation [c]). However, if there is an additional increase of tidal range as MSL rises, then flooding will be more extreme, both with storm surge and without (situation [d]).

If tidal evolution related to MSL variability is present, then flood risk cannot accurately be assessed via superposition of present-day tides and surge onto a higher baseline sea-level, as such predictions would be insufficient at locations with a high tidal sensitivity to water levels. Long-term trends of tides and MSL can give a picture of the “slow and steady change” that will be most relevant for the future of coastal health, such as the unrecoverable loss of low-lying population zones such as estuaries under higher baseline MSL. On the other hand, short-term variabilities can indicate where “quick and sudden change” is important, which may increase the intensity of major storms as well as increasing the frequency of lower-impact yet more frequent high-water events (such as nuisance flooding) that can yield a

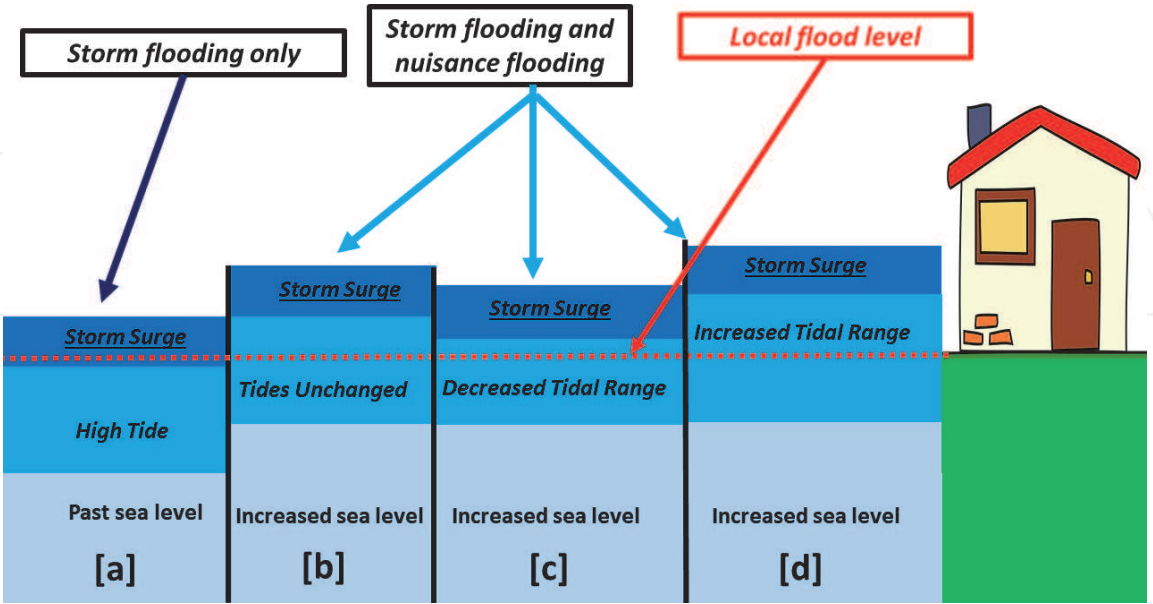


Figure 19. Simple cartoon showing the effect of nuisance flooding under four situations [9]. In the past, when sea levels were lower, it would take a large storm surge to cause nuisance flooding (situation [a]), but more recently, as sea levels have risen, nuisance flooding may happen at high tide (situation [b]). If tidal range are damped as MSL rises, then situation [c] will arise, where nuisance flooding is still present, but not as much as in situation [b]. If tidal amplitudes also increase as MSL increases, then flooding will be particularly extreme (situation [d]). The red dashed line indicates the local flood level, which is only exceeded by storm surge in the past (situation [a]), but under modern MSL conditions is exceeded to varying degrees in situations [b], [c], and [d].

cumulative degradation of coastal areas. Therefore, both tides and MSL should be considered to fully quantify future water level changes in coastal areas, and a regional-to-local approach is prescribed.

6. Conclusions

This chapter has strived to summarize the salient features of a suite of past studies [7–11] that have analyzed the issue of changing tidal evolution that is correlated with MSL variability, both of which are likely related to climate-change related factors. It has been demonstrated that these tidal changes are likely to have the greatest effect on coastal locations, especially estuarine regions, which are often highly developed, densely populated, and environmentally sensitive. Overall, in both the Pacific and Atlantic, over 90% of all locations surveyed show a significant TAC in at least one tidal constituent, and around one-third of all locations have a significant δ -HAT.

In general, coastal inundation is associated with peak water level, not mean sea level, and depends on the combined effects of tides, storm surge, sea-level variability, inland precipitation, river flow, and other factors which may lead to increases in extreme water level exceedance probabilities. MSL rise can affect the tidal dynamics directly, or the reasons for the observed changes can be related to secondary mechanisms, including, but not limited to: river flow, changing bed friction due to harbor development and other causes, barotropic friction effects, heat content, buoyancy, stratification, mixing and eddy viscosity, ocean currents, waves, storm surge, and indeed, any source of water or energy input.


Here, the effects of tidal evolution, and the impacts of these changes on nuisance flooding have been described. Identifying connections and correlations between tidal range and MSL is critical for making reliable predictions of coastal water levels and inundation risk. When combined with storm surge, larger tides and higher MSL may amplify flood risk, coastal inundation, damage to infrastructure, and population displacement. Even without the consideration of storm surge, changes in tides and sea-levels may lead to more occurrences of nuisance flooding.

Author details

Adam Thomas Devlin* and Jiayi Pan
School of Geography and Environment, Jiangxi Normal University, Nanchang,
Jiangxi, China

*Address all correspondence to: atdevin@jxnu.edu.cn; phlux1@gmail.com

IntechOpen

© 2020 The Author(s). Licensee IntechOpen. This chapter is distributed under the terms of the Creative Commons Attribution License (<http://creativecommons.org/licenses/by/3.0>), which permits unrestricted use, distribution, and reproduction in any medium, provided the original work is properly cited. 

References

- [1] Gutzwiller MC. Moon-Earth-Sun: The oldest three-body problem. *Reviews of Modern Physics*. 1998;**70**(2):589
- [2] Church JA, White NJ. Sea level rise from the late 19th to the early 21st century. *Surveys in Geophysics*. 2011;**32**(4–5):585-602. DOI: 10.1007/s10712-011-9119-1
- [3] Kopp RE, Kemp AC, Bittermann K, Horton BP, Donnelly JP, Gehrels WR, et al. Temperature-driven global sea-level variability in the Common Era. *Proceedings of the National Academy of Sciences*. 2016;**113**(11):E1434-E1441
- [4] Domingues CM, Church JA, White NJ, Gleckler PJ, Wijffels SE, Barker PM, et al. Improved estimates of upper-ocean warming and multi-decadal sea level rise. *Nature*. 2008;**453**(7198):1090. DOI: 10.1038/nature07080
- [5] Moftakhari HR, AghaKouchak A, Sanders BF, Matthew RA. Cumulative hazard: The case of nuisance flooding. *Earth's Future*. 2017;**5**(2):214-223. DOI: 10.1002/2016EF000494
- [6] Moftakhari HR, AghaKouchak A, Sanders BF, Feldman DL, Sweet W, Matthew RA, et al. Increased nuisance flooding along the coasts of the United States due to sea level rise: Past and future. *Geophysical Research Letters*. 2015;**42**(22):9846-9852. DOI: 10.1002/2015GL066072
- [7] Devlin AT, Jay DA, Talke SA, Zaron E. Can tidal perturbations associated with sea level variations in the western Pacific Ocean be used to understand future effects of tidal evolution? *Ocean Dynamics*. 2014;**64**(8):1093-1120. DOI: 10.1007/s10236-014-0741-6
- [8] Devlin AT, Jay DA, Zaron ED, Talke SA, Pan J, Lin H. Tidal variability related to sea level variability in the Pacific Ocean. *Journal of Geophysical Research-Oceans*. 2017;**122**(11):8445-8463. DOI: 10.1002/2017JC013165
- [9] Devlin AT, Jay DA, Talke SA, Zaron ED, Pan J, Lin H. Coupling of sea level and tidal range changes, with implications for future water levels. *Scientific Reports*. 2017;**7**(1):17021. DOI: 10.1038/s41598-017-17056-z
- [10] Devlin AT, Pan J, Lin H. Extended spectral analysis of tidal variability in the North Atlantic Ocean. *Journal of Geophysical Research-Oceans*. 2019;**124**(1):506-526
- [11] Devlin AT, Pan J, Lin H. Tidal variability in the Hong Kong region. *Ocean Science*. 2019;**15**(4):853-864
- [12] Church JA, White NJ. A 20th century acceleration in global sea-level rise. *Geophysical Research Letters*. 2006;**33**(1). DOI: 10.1029/2005GL024826
- [13] Nicholls RJ, Cazenave A. Sea-level rise and its impact on coastal zones. *Science*. 2010;**328**(5985):1517-1520. DOI: 10.1126/science.1185782
- [14] Nerem RS, Chambers DP, Choe C, Mitchum GT. Estimating mean sea level change from the TOPEX and Jason altimeter missions. *Marine Geodesy*. 2010;**33**(S1):435-446. DOI: 10.1080/01490419.2010.491031
- [15] Slangen AB, Church JA, Agosta C, Fettweis X, Marzeion B, Richter K. Anthropogenic forcing dominates global mean sea-level rise since 1970. *Nature Climate Change*. 2016;**6**(7):701-705. DOI: 10.1038/nclimate2991
- [16] Dangendorf S, Marcos M, Wöppelmann G, Conrad CP, Frederikse T, Riva R. Reassessment of 20th century global mean sea level rise. *Proceedings of the National Academy of Sciences*. 2017;**114**(23):5946-5951

- [17] Woodworth PL, White NJ, Jevrejeva S, Holgate SJ, Church JA, Gehrels WR. Evidence for the accelerations of sea level on multi-decade and century timescales. *International Journal of Climatology: A Journal of the Royal Meteorological Society*. 2009;**29**(6): 777-789. DOI: 10.1002/joc.1771
- [18] Jevrejeva S, Grinsted A, Moore JC, Holgate S. Nonlinear trends and multiyear cycles in sea level records. *Journal of Geophysical Research: Oceans*. 2006;**111**(C9)
- [19] Sallenger AH Jr, Doran KS, Howd PA. Hotspot of accelerated sea level rise on the Atlantic coast of North America. *Nature Climate Change*. 2012;**2**(12): 884-888
- [20] Merrifield MA, Merrifield ST, Mitchum GT. An anomalous recent acceleration of global sea level rise. *Journal of Climate*. 2009;**22**(21):5772-5781. DOI: 10.1175/2009JCLI2985.1
- [21] Merrifield MA. A shift in western tropical Pacific Sea level trends during the 1990s. *Journal of Climate*. 2011;**24** (15):4126-4138. DOI: 10.1175/2011JCLI3932.1
- [22] Peyser CE, Yin J. Interannual and decadal variability in Tropical Pacific Sea level. *Water*. 2017;**9**(6):402. DOI: 10.3390/w9060402
- [23] Bromirski PD, Miller AJ, Flick RE, Auad G. Dynamical suppression of sea level rise along the Pacific Coast of North America: Indications for imminent acceleration. *Journal of Geophysical Research*. 2011;**116**: C07005. DOI: 10.1029/2010JC006759
- [24] Cartwright DE, Tayler RJ. New computations of the tide-generating potential. *Geophysical Journal of the Royal Astronomical Society*. 1971;**23**:45-74. DOI: 10.1111/j.1365-246X.1971.tb01803.x
- [25] Haigh ID, Wijeratne EMS, MacPherson LR, Pattiaratchi CB, Mason MS, Crompton RP, et al. Estimating present day extreme water level exceedance probabilities around the coastline of Australia: tides, extra-tropical storm surges and mean sea level. *Climate Dynamics*. 2014;**42**(1-2): 121-138
- [26] Müller M, Arbic BK, Mitrovica JX. Secular trends in ocean tides: Observations and model results. *Journal of Geophysical Research-Oceans*. 2011; **116**(C5). DOI: 10.1029/2010JC006387
- [27] Woodworth PL. A survey of recent changes in the main components of the ocean tide. *Continental Shelf Research*. 2010;**30**(15):1680-1691. DOI: 10.1016/j.csr.2010.07.002
- [28] Mawdsley RJ, Haigh ID, Wells NC. Global secular changes in different tidal high water, low water and range levels. *Earth's Future*. 2015;**3**(2):66-81
- [29] Cartwright DE. Secular changes in the oceanic tides at Brest, 1711-1936. *Geophysical Journal International*. 1972; **30**(4):433-449. DOI: 10.1.1.867.2468
- [30] Proudman J, Doodson AT. V. The principal constituent of the tides of the North Sea. *Philosophical Transactions of the Royal Society of London. Series A, Containing Papers of a Mathematical or Physical Character*. 1924;**224**(616-625): 185-219
- [31] Amin M. On perturbations of harmonic constants in the Thames Estuary. *Geophysical Journal of the Royal Astronomical Society*. 1983;**73**(3): 587-603. DOI: 10.1111/j.1365-246X.1983.tb03334.x
- [32] Bowen AJ, Gray DA. The tidal regime of the River Thames; long-term trends and their possible causes. *Philosophical Transactions of the Royal Society of London A*. 1972;**272**(1221): 187-199. DOI: 10.1098/rsta.1972.0045

- [33] Vellinga NE, Hoitink AJF, van der Vegt M, Zhang W, Hoekstra P. Human impacts on tides overwhelm the effect of sea level rise on extreme water levels in the Rhine–Meuse delta. *Coastal Engineering*. 2014;**90**:40-50. DOI: 10.1016/j.coastaleng.2014.04.005
- [34] Chernetsky AS, Schuttelaars HM, Talke SA. The effect of tidal asymmetry and temporal settling lag on sediment trapping in tidal estuaries. *Ocean Dynamics*. 2010;**60**:1219-1241. DOI: 10.1007/s10236-010-0329-8
- [35] Familkhalili R, Talke SA. The effect of channel deepening on tides and storm surge: A case study of Wilmington, NC. *Geophysical Research Letters*. 2016;**43** (17):9138-9147. DOI: 10.1002/2016GL069494
- [36] Jay DA, Leffler K, Degens S. Long-term evolution of Columbia River tides. *ASCE Journal of Waterway, Port, Coastal, and Ocean Engineering*. 2011; **137**:182-191. DOI: 10.1061/(ASCE)WW.1943- 5460.0000082
- [37] Colosi JA, Munk W. Tales of the venerable Honolulu tide gauge. *Journal of Physical Oceanography*. 2006;**36**(6): 967-996. DOI: 10.1175/JPO2876.1
- [38] Müller M, Cherniawsky JY, Foreman MGG, Storch JS. Global M_2 internal tide and its seasonal variability from high resolution ocean circulation and tide modeling. *Geophysical Research Letters*. 2012;**39**(19). DOI: 10.1029/2012GL053320
- [39] Jay DA. Evolution of tidal amplitudes in the eastern Pacific Ocean. *Geophysical Research Letters*. 2009;**36**: L04603. DOI: 10.1029/2008GL036185
- [40] Ray RD. Secular changes of the M_2 tide in the Gulf of Maine. *Continental Shelf Research*. 2006;**26**(3):422-427. DOI: 10.1016/j.csr.2005.12.005
- [41] Ray RD. Secular changes in the solar semidiurnal tide of the Western North Atlantic Ocean. *Geophysical Research Letters*. 2009;**36**(19). DOI: 10.1029/2009GL040217
- [42] Feng X, Tsimplis MN. Sea level extremes at the coasts of China. *Journal of Geophysical Research-Oceans*. 2014; **119**(3):1593-1608. DOI: 10.1002/2013JC009607
- [43] Feng X, Tsimplis MN, Woodworth PL. Nodal variations and long-term changes in the main tides on the coasts of China. *Journal of Geophysical Research-Oceans*. 2015;**120**(2):1215-1232. DOI: 10.1002/2014JC010312
- [44] Rasheed AS, Chua VP. Secular trends in tidal parameters along the coast of Japan. *Atmosphere-Ocean*. 2014;**52**(2):155-168. DOI: 10.1080/07055900.2014.886031
- [45] Zaron ED, Jay DA. An analysis of secular change in tides at open-ocean sites in the Pacific. *Journal of Physical Oceanography*. 2014;**44**(7):1704-1726. DOI: 10.1175/JPO-D-13-0266.1
- [46] Arbic BK, Karsten RH, Garrett C. On tidal resonance in the global ocean and the back-effect of coastal tides upon open-ocean tides. *Atmosphere-Ocean*. 2009;**47**(4):239-266. DOI: 10.3137/OC311.2009
- [47] Skiba AW, Zeng L, Arbic BK, Müller M, Godwin WJ. On the resonance and shelf/open-ocean coupling of the global diurnal tides. *Journal of Physical Oceanography*. 2013; **43**(7):1301-1324. DOI: 10.1175/JPO-D-12-054.1
- [48] Arbic BK, Garrett C. A coupled oscillator model of shelf and ocean tides. *Continental Shelf Research*. 2010;**30**(6): 564-574. DOI: 10.1016/j.csr.2009.07.008
- [49] Pugh DT. *Tides, Surges and Mean Sea Level: A Handbook for Engineers and Scientists*. Chichester: Wiley; 1987. 472pp. ISBN: 978-0471915058

- [50] Müller M. The influence of changing stratification conditions on barotropic tidal transport and its implications for seasonal and secular changes of tides. *Continental Shelf Research*. 2012;**47**:107-118. DOI: 10.1016/j.csr.2012.07.003
- [51] Kang SK, Chung JY, Lee SR, Yum KD. Seasonal variability of the M2 tide in the seas adjacent to Korea. *Continental Shelf Research*. 1995;**15**(9): 1087-1113
- [52] Guo L, van der Wegen M, Jay DA, Matte P, Wang ZB, Roelvink D, et al. River-tide dynamics: Exploration of nonstationary and nonlinear tidal behavior in the Yangtze River estuary. *Journal of Geophysical Research-Oceans*. 2015;**120**(5):3499-3521. DOI: 10.1002/2014JC010491
- [53] Hootink AJF, Jay DA. Tidal river dynamics: Implications for deltas. *Reviews of Geophysics*. 2016;**54**(1): 240-272
- [54] Pugh DT. Changing sea levels. In: *Effects of Tides, Weather and Climate*. Cambridge, UK: Cambridge University Press; 2004. 280pp. ISBN: 978-0521532181
- [55] Pickering MD, Wells NC, Horsburgh KJ, Green JAM. The impact of future sea-level rise on the European Shelf tides. *Continental Shelf Research*. 2012;**35**:1-15
- [56] Holleman RC, Stacey MT. Coupling of sea level rise, tidal amplification, and inundation. *Journal of Physical Oceanography*. 2014;**44**(5):1439-1455. DOI: 10.1175/JPO-D-13-0214.1
- [57] Holgate SJ, Woodworth PL. Evidence for enhanced coastal sea level rise during the 1990s. *Geophysical Research Letters*. 2004;**31**(7)
- [58] Leffler KE, Jay DA. Enhancing tidal harmonic analysis: Robust (hybrid L1/L2) solutions. *Continental Shelf Research*. 2009;**29**(1):78-88. DOI: 10.1016/j.csr.2008.04.011
- [59] Pawlowicz R, Beardsley B, Lentz S. Classical tidal harmonic analysis including error estimates in MATLAB using T_TIDE. *Computers and Geosciences*. 2002;**28**(8):929-937. DOI: 10.1016/S0098-3004(02)00013-4
- [60] Cartwright DE, Edden AC. Corrected tables of tidal harmonics. *Geophysical Journal International*. 1973; **33**(3):253-264. DOI: 10.1111/j.1365-246X.1973.tb03420.x
- [61] Woodworth PL, Hunter JR, Marcos M, Caldwell P, Menéndez M, Haigh I. Towards a global higher-frequency sea level dataset. *Geoscience Data Journal*. 2016;**3**(2):50-59. DOI: 10.1002/gdj3.42
- [62] Egbert GD, Erofeeva SY. Efficient inverse modeling of barotropic ocean tides. *Journal of Atmospheric and Oceanic Technology*. 2002;**19**(2):183-204. DOI: 10.1175/1520-0426(2002)019<0183: EIMOBO>2.0.CO
- [63] Egbert GD, Erofeeva SY. OTIS: The OSU Tidal Inversion Software TPX07. 2. College of Oceanic and Atmospheric Sciences, Oregon State University. 2010. Available from: <http://volkov.oce.orst.edu/tides/otis.html>
- [64] Devlin AT, Zaron ED, Jay DA, Talke SA, Pan J. Seasonality of tides in Southeast Asian waters. *Journal of Physical Oceanography*. 2018;**48**(5): 1169-1190
- [65] Mudersbach C, Wahl T, Haigh ID, Jensen J. Trends in high sea levels of German North Sea gauges compared to regional mean sea level changes. *Continental Shelf Research*. 2013;**65**:111-120. DOI: 10.1016/j.csr.2013.06.016
- [66] Sweet WV, Park J. From the extreme to the mean: Acceleration and tipping points of coastal inundation

from sea level rise. *Earth's Future*. 2014; **2**(12):579-600

[67] Calafat FM, Wahl T, Lindsten F, Williams J, Frajka-Williams E. Coherent modulation of the sea-level annual cycle in the United States by Atlantic Rossby waves. *Nature Communications*. 2018;**9** (1):2571

[68] Moftakhari HR, AghaKouchak A, Sanders BF, Allaire M, Matthew RA. What is nuisance flooding? Defining and monitoring an emerging challenge. *Water Resources Research*. 2018;**54**(7): 4218-4227

[69] Suarez P, Anderson W, Mahal V, Lakshmanan TR. Impacts of flooding and climate change on urban transportation: A systemwide performance assessment of the Boston Metro Area. *Transportation Research Part D: Transport and Environment*. 2005;**10**(3):231-244. DOI: 10.1016/j.trd.2005.04.007

[70] Cherqui F, Belmeziti A, Granger D, Sourdril A, Le Gauffre P. Assessing urban potential flooding risk and identifying effective risk-reduction measures. *Science of the Total Environment*. 2015;**514**:418-425. DOI: 10.1016/j.scitotenv.2015.02.027

[71] Ten Veldhuis JAE, Clemens FHLR, Sterk G, Berends BR. Microbial risks associated with exposure to pathogens in contaminated urban flood water. *Water Research*. 2010;**44**(9):2910-2918. DOI: 10.1016/j.watres.2010.02.009

[72] Vandenberg-Rodes A, Moftakhari HR, AghaKouchak A, Shahbaba B, Sanders BF, Matthew RA. Projecting nuisance flooding in a warming climate using generalized linear models and Gaussian processes. *Journal of Geophysical Research-Oceans*. 2016;**121** (11):8008-8020

[73] Ray RD, Foster G. Future nuisance flooding at Boston caused by

astronomical tides alone. *Earth's Future*. 2016;**4**(12):578-587. DOI: 10.1002/2016EF000423

[74] Arns A, Dangendorf S, Jensen J, Bender J, Talke SA, Pattiaratchi C. Sea level rise induced amplification of coastal protection design heights. *Nature Scientific Reports*. 2017;**7**:40171. DOI: 10.1038/srep40171